# Homeodomain proteins hierarchically specify neuronal diversity and synaptic connectivity

Chundi Xu[1]*, Tyler B. Ramos[1], Ed M. Rogers[2], Michael B. Reiser[2], Chris Q. Doe[1]

[1]Institute of Neuroscience, Howard Hughes Medical Institute, University of Oregon; Eugene, OR 97403, USA
[2]Janelia Research Campus, Howard Hughes Medical Institute, 19700 Helix Drive, Ashburn, VA, USA.

*Corresponding author. Email: cxu3@uoregon.edu

## Summary

The brain generates diverse neuron types which express unique homeodomain transcription factors (TFs) and assemble into precise neural circuits. Yet a mechanistic framework is lacking for how homeodomain TFs specify both neuronal fate and synaptic connectivity. We use *Drosophila* lamina neurons (L1-L5) to show the homeodomain TF Brain-specific homeobox (Bsh) is initiated in lamina precursor cells (LPCs) where it specifies L4/L5 fate and suppresses homeodomain TF Zfh1 to prevent L1/L3 fate. Subsequently, Bsh activates the homeodomain TF Apterous (Ap) in L4 in a feedforward loop to express the synapse recognition molecule DIP-β, in part by Bsh direct binding a *DIP-β* intron. Thus, homeodomain TFs function hierarchically: primary homeodomain TF (Bsh) first specifies neuronal fate, and subsequently acts with secondary homeodomain TF (Ap) to activate DIP-β, thereby generating precise synaptic connectivity. We speculate that hierarchical homeodomain TF function may represent a general principle for coordinating neuronal fate specification and circuit assembly.

## Keywords

neuronal fate, neuronal diversity, synaptic connectivity, homeodomain transcription factor, feedforward loop, Bsh, Apterous, Zfh1, Pdm3, lamina, DIP-β

## Introduction

Our ability to percieve the world requires a diverse array of neuron types with precise connectivity. Each neuron type is generated in a stepwise manner. Transient spatial and temporal cues act in progenitors to specify neuronal fate (Bayraktar and Doe, 2013; Doe, 2017; Erclik et al., 2017; Holguera and Desplan, 2018; Sen et al., 2019), followed by neuron type-specific TFs expressed in immature neurons that establish unique neuronal synaptic connectivity (Cubelos et al., 2010; De Marco Garcia and Jessell, 2008; Enriquez et al., 2015; Hasegawa et al., 2013; Hobert and Kratsios, 2019; Reilly et al., 2020; Thor and Thomas, 1997). These steps are intimately connected, yet our

knowledge of how they are coordinately regulated remains unclear. Work in mouse ventral neural tube found that progenitors display discrete homeodomain TFs expression domains which generate specific neuron types (Briscoe et al., 2000; Ericson et al., 1997). In *C. elegans*, each of the 118 neuron classes expresses a unique combination of homeodmain TFs which control neuron type-specific neurotransmitter identity and connectivity (Hobert, 2021; Pereira et al., 2015; Reilly et al., 2020). These findings lead to the hypothesis that homeodomain TFs may sequentially specify neuronal fate and circuit assembly. Here we test this hypothesis in *Drosophila*, asking the following questions. Do progenitor and neuronal homeodomain TFs function hierarchically or in parallel? Do homeodomain TFs that specify neuronal fate also regulate synaptic connectivity? Do sequentially acting homeodomain TFs act in a feed-forward gene regulatory motif?

To address these questions, we chose lamina neurons within the *Drosophila* visual system as a model. During late larval and early pupal stages, LPCs give rise to five types of lamina neurons (L1-L5). The core motion detection neurons L1-L3 receive direct synaptic inputs from photoreceptors and mediate visual motion detection (Meinertzhagen and O'Neil, 1991; Rivera-Alba et al., 2011; Silies et al., 2013; Tuthill et al., 2013), whereas L4 and L5 receive synaptic inputs from L2 and L1 respectively, and their function is currently unclear (Meinertzhagen and O'Neil, 1991; Rivera-Alba et al., 2011; Silies et al., 2013; Tuthill et al., 2013). The cell bodies of each lamina neuron are localized in a layer-specific manner (Tan et al., 2015). L2/L3 cell bodies are intermingled in the most distal layer while L1, L4, and L5 form distinct layers progressively more proximal. Each lamina neuron expresses unique TF markers. L1, L2 and L3 neurons express Svp, Bab2 and Erm respectively (Tan et al., 2015). L4 and L5 neurons express a combination of homeodomain TFs Bsh/Ap and Bsh/Pdm3, respectively (Hasegawa et al., 2013; Tan et al., 2015). Here we focus on homeodomain TF combinations Bsh/Ap in L4 and Bsh/Pdm3 in L5 neurons.

## Results

### Sequential initiation of homeodomain TFs during lamina neurogenesis

L4 and L5 neurons are generated by a subset of LPCs during late larval and early pupal stages, but is unknown exactly when expression of Bsh, Ap or Pdm3 are initiated. To address this question, we identified the Tailless (Tll) TF as a novel marker for LPCs (Figures 1A-1A'' and S1A-S1A'''). Indeed, Tll and the neuronal marker Elav have precisely complementary high-level expression, validating Tll as an LPC marker (Figures 1A-1A'' and 1F). Importantly, we found that Bsh was first detected in a subset of LPCs (Figures 1B-1B'''). In contrast, Ap was first detected in L4 neurons, and Pdm3 was first detected in L5 neurons (Figures 1C-1D''' and 1G). Ap and Pdm3 were never detected in LPCs or newborn L4 or L5 neurons (Figures 1C-1D'''). Lamina neuron expression of Bsh, Ap and Pdm3 was maintained into the adult (Figures 1E-1E''), consistent with a potential role as terminal selectors in maintaining neuron identity (Deneris and Hobert, 2014; Serrano-Saiz et al., 2018). We conclude that Bsh expression is initiated in LPCs and maintained in neurons and subsequently Ap and Pdm3 are initiated and maintained in neurons. Due to its earlier expression we

refer to Bsh as a primary homeodomain TF and due to their later expression, we refer to Ap and Pdm3 as secondary homeodomain TFs.

**Bsh activates Ap/Pdm3 expression and specifies L4/L5 neuronal fate**

Bsh is expressed prior to Ap and Pdm3, raising the possibility that Bsh activates Ap and Pdm3 expression. To test whether Bsh in LPCs is required for Ap/Pdm3 expression, we used the R27G05-Gal4 driver to target Bsh RNAi to LPCs. R27G05-Gal4 is expressed in all LPCs and turned off in lamina neurons, though the myristoylated-GFP reporter can be detected in the cell bodies of neurons until ~66 hours after pupa formation (APF) (Figures S1B-S1F). As expected, Bsh-knockdown (KD) eliminates Bsh expression in LPCs and newborn neurons (Figures 2A-2B''). Bsh remains undetectable in the lamina neurons in the late pupa and adult, despite lack of RNAi expression, which indicates that Bsh expression is unable to reinitiate in neurons if Bsh is lost in LPCs (Figures 2C-2D'' and S2A-S2B'''). Importantly, we found that Ap and Pdm3 were mostly undetectable when knocking down Bsh (Figures 2E-2H, S2A-S2B''', S2E, and S2F). Note that the unexpected ectopic Ap expression in L5 is caused by the R27G05-Gal4 line, but this does not affect our experiments (Figures 2E-2F''). We conclude that Bsh in LPCs is required for Ap and Pdm3 expression.

Homeodomain TFs Bsh/Ap and Bsh/Pdm3 are L4 and L5 markers respectively. Bsh, Ap and Pdm3 are almost all absent in Bsh-KD which indicates that L4 and L5 neuronal fate are lost. Consistent with the Bsh-KD phenotype, we found similar results using a Bsh Crispr/Cas9 knock out (KO) (Figures S2C-S2D''' and S2G-S2I). Taken together, we conclude that the primary homeodomain TF Bsh is required to drive expression of the secondary homeodomain TFs Ap and Pdm3 and specify L4 and L5 neuronal fates (Figure 2J).

To determine if Bsh was continuously required for Ap expression in L4, we used Bsh-KO in immature L4 neurons. We found that Bsh-KO eliminates Bsh expression (as expected), but there are no changes in Ap expression (Figures S3 and S4); this suggests that Ap undergoes positive autoregulation after its initiation, rendering it independent of Bsh. Autoregulation is a common feature of homeodomain TFs (Leyva-Díaz and Hobert, 2019). We conclude that Bsh is not required to maintain Ap expression in L4 neurons.

**Bsh suppresses L1/L3 neuronal fate**

We next asked whether Bsh-KD resulted in the death of L4/L5, or if they are transformed into another lamina neuron identity. We found that the number of lamina neurons remains normal in Bsh-KD, indicating that L4/L5 have assumed a different cell fate (Figure 2I). To test for ectopic generation of another lamina neuron type we assayed expression of Svp (L1), Bab2 (L2) and Erm (L3). We found that Bsh-KD led to ectopic expression of the L1 and L3 markers Svp and Erm in the positions normally occupied by L4/L5 cell bodies (Figures 3A-3D). Notably, we never saw cell bodies co-expressing Erm and Svp, which indicates that the absence of Bsh

generates ectopic L1 and L3 neuron fate but not a hybrid neuronal fate. In contrast, the L2 marker Bab2 was unaffected by Bsh-KD (Figures S5A-S5B''', S5F, and S5G). We conclude that the primary homeodomain TF Bsh promotes L4/L5 fate and suppresses L1/L3 neuronal fate, thereby increasing lamina neuronal diversity (Figure 3K).

Although we have shown that Bsh-KD generates L1/L3 neurons instead of L4/L5 neurons, it was not clear if this was a one-to-one switch, e.g. L4>L3 and L5>L1. To identify the neuronal fate generated at the expense of L5 fate following Bsh-KD, we used Bsh-LexA>LexAop-GFP to label Bsh+ LPCs plus L5 neurons (Figures S5C-S5D'''). We found that Bsh-KD generated GFP+ neurons (normally L5) that lacked the L5 marker Pdm3 and instead showed ectopic expression of the L1 marker Svp and L1-like morphology (Figures 3E-3J). Interestingly, some of the GFP+Svp+ neurons had cell bodies displaced from the L5 layer into the L1 layer, which suggests that L1 neurons may actively seek out their appropriate settling layer (Figures 3F-3F''). Because Bsh-KD transforms L5 into L1 identity, the remaining neurons must show an L4 to L3 transformation. This is consistent with the previous report showing transformation of L4 to L3 morphology in *Bsh* mutant clones, though L5 neurons were found to transform to glia cells using L5-Gal4 (Hasegawa et al., 2013), although this may not faithfully label L5 after cell fate transformation. We conclude that Bsh is required to specify L4/L5 identity and suppress L3/L1 identity, respectively.

Bsh-KD in LPCs results in a loss of Ap expression and ectopic L1/L3 marker expression. To exclude the possibility that Bsh represses L1/L3 fate through Ap, we knocked down Ap expression using R27G05-Gal4 driver, which is expressed in LPCs. As expected, Ap-KD eliminates Ap initiation in L4 neurons (Figures S6A-S6C). Furthermore, Ap remained undetectable in lamina neurons in adult, this indicates that Ap expression is unlikely able to reinitiate if normal initiation is lost (Figures S6D-S6F). Importantly, loss of Ap did not affect Bsh expression in L4, and did not lead to ectopic expression of L1/L3 lamina neuron markers (Figure S7). Taken together, we conclude that only the primary homeodomain TF Bsh, but not the secondary homeodomain TF Ap, is required to repress L1/L3 lamina neuronal fate (Figure 3K).

**Bsh represses Zfh1 to suppress L1/L3 neuronal fate**

How does the primary homeodomain TF Bsh repress L1 and L3 neuronal fates? Following Bsh-KD, the L1 marker Svp was not detected in the GFP+ LPCs (Figures S5E-S5F'''). This temporal delay in ectopic Svp expression suggests that Bsh acts through an intermediate to repress Svp and Erm expression. To find this intermediate TF, we screened published RNA-seq data (Tan et al., 2015) and found the homeodomain TF Zfh1 was specifically expressed in L1 and L3. We validated the RNA-seq results by showing that Zfh1 is present in all LPCs before becoming restricted to L1 and L3 neurons (Figures 4A-4B'''). To determine if Zfh1 is required for L1 and L3 neuronal fate, we used RNAi to perform Zfh1-KD in LPCs. As expected, Zfh1-KD significantly decreased Zfh1expression in all LPCs and neurons, and Zfh1 remained undetectable at 3-4d APF (Figures 4C-4D'' and S8A-S8D). Importantly, Zfh1-KD resulted in a loss of Svp+ L1 and Erm+ L3 neurons which suggests that

Zfh1 is required for L1 and L3 neuronal identity (Figures 4C-4F). In addition, the decreased number of lamina neurons and Bsh+ L4 and L5 neurons in Zfh1-KD suggests a potential role for Zfh1 in LPCs in regulating lamina neurogenesis (Figures S8E-S8J). Furthermore, the Bsh-KD resulted in ectopic expression of Zfh1 in the L4/L5 cell body layers and in GFP+ neurons (normally L5) (Figures 4G-4J and S8K-S8M). We propose that the primary homeodomain TF Bsh represses Zfh1 (thereby limiting L1/L3 specification) and specifies L4 and L5 neuron identity; absence of Bsh results in ectopic L1/L3 at the expense of L4/L5 (Figure 4K).

**Bsh and Ap are in a feed-forward loop that drives expression of the synapse recognition molecule DIP-β**

In other systems, homeodomain TFs control the acquisition of distinct aspects of neuronal identity, including cell surface proteins involved in circuit formation (Hobert and Kratsios, 2019). We previously showed that the cell surface protein DIP-β is specifically detected in L4 and required for proper L4 circuit connectivity (Xu et al., 2019). Here we ask whether Bsh and/or Ap are required for L4 expression of DIP-β. We found that Bsh-KO in L4 neurons resulted in a strong decrease in DIP-β levels (Figures 5A-5D and S3). Furthermore, using the STaR method (Chen et al., 2014; Xu et al., 2019) we found that L4 primary dendrite length and presynaptic Bruchpilot (Brp) puncta in the proximal lamina were both decreased following Bsh-KO (Figures 5E-5I), which is distinct from the DIP-β-KD phenotype (Xu et al., 2019). We conclude that Bsh acts in L4 to promote DIP-β expression, neuron morphology and connectivity.

To test whether Ap controls DIP-β expression in L4, we knocked down Ap using RNAi prior to its time of initiation in L4 neurons, and observed a strong decrease in DIP-β levels in L4 neurons (Figures 5J-5M and S6A-S6C). We next combined the STaR method with Ap-shRNA, resulting in loss of Ap expression in L4 at 2d APF and a strong decrease in DIP-β levels in L4 neurons (Figure S9). Importantly, Ap-KD in L4 neurons increased Brp puncta in the distal/proximal lamina and increased the length of L4 primary dendrites (Figures 5N-5R). This phenotype is similar to the DIP-β-KD phenotype (Xu et al., 2019), suggesting that Ap might regulate L4 morphology and synaptic connectivity primarily via DIP-β. Together, our data shows that Bsh activates Ap, and then Bsh and Ap act together in a feedforward loop to drive DIP-β expression and regulate L4 morphology and synaptic connectivity (Figures 5S).

***DIP-β* is a direct target of Bsh**

To investigate whether the synapse recognition molecule *DIP-β* gene is a direct target of homeodomain TF Bsh, we profiled Bsh targets with precise spatial and temporal control: only in L4 neurons at the time of synapse formation. To do this we used Targeted DamID (TaDa), which can be used to identify Bsh DNA-binding sites across the genome (Figure 6A; see Methods). We generated a Bsh:Dam transgenic fly line using the FlyORF-TaDa system (Aughey et al., 2021), and verified that the Bsh:Dam fusion protein was functional (Figures S10B-S10D). We

expressed Bsh:Dam in L4 neurons using 31C06-Gal4 (Figures S10A-S10A"). We performed three biological replicates which had high reproducibility (Figures 6B and 6C). Importantly, Bsh:Dam showed strong binding peaks in L4 neurons within the first intron of the *DIP-β* gene (Figures 6E and 6F). This intron is also within open chromatin (Figures 6G and 6H). Consistent with Bsh:Dam binding in the *DIP-β* intron, PWMScan identified a single Bsh DNA-binding motif (CIS-BP motif M1089_1.02) within the first intron of *DIP-β* gene (Figure 6D; see Methods). Additional evidence for the functional importance of the *DIP-β* first intron is that the Ecdysone receptor (EcR), which controls the temporal expression of *DIP-β* in L4 neurons, also has a DNA-binding motif in the *DIP-β* first intron (Jain et al., 2022). Taken together, our data shows that the Bsh transcription factor binds directly to the *DIP-β* first intron in L4 neurons at the time of synapse formation.

**Bsh+ L4/L5 are required for normal visual sensitivity**

Bsh is required to specify L4/L5 neuronal fate and generate lamina neuronal diversity (L1-L3 -> L1-L5), raising the hypothesis that lack of Bsh may compromise lamina function. To test this, we used an apparatus (the Fly Vision Box) that integrates multiple assays including visual motion (Zhu et al., 2009), phototaxis (Benzer, 1967) and spectral preference (Gao et al., 2008) in flies walking in transparent tubes (Figure 7A; see Methods). We found that Bsh-KD adults lacking most L4/L5 neurons showed a reduced response to a high-speed stimulus, suggesting weakened sensitivity to visual motion (Figures 7B, S2B, and S11). When tested with both UV and green LEDs, the Bsh-KD flies had reduced phototaxis to both dim and bright lights, suggesting less sensitivity to both UV and green lights. Interestingly, the Bsh-KD flies exhibited larger responses towards bright UV illumination in the spectral preference assay (Figures 7C and 7D). This apparent attraction to bright UV light may result from more weakened sensitivity to the green light, which may be expected since L4 and L5 are indirect R1-6 targets (Takemura et al., 2015). Taken together, we conclude that the primary homeodomain TF Bsh is required to generate lamina neuronal diversity and normal visual behavior (Figure 7E).

**Discussion**

Homeodomain TFs are expressed in a unique combination in each neuron type in the *C. elegans* nervous system and function as terminal selectors to control the expression of cell-type-specific gene batteries (Hobert, 2021; Reilly et al., 2020). Here we generalize and move this "terminal selectors" model one step further by discovering the hierarchical function of homeodomain TFs in coupling neuronal fate specification and synaptic connectivity in *Drosophila* (Figure 7E). First, a primary homeodomain TF (Bsh) activates a secondary homeodomain TF; Ap in L4 neurons or Pdm3 in L5 neurons. Second, only the primary homeodomain TF (Bsh) but not the secondary (Ap) is required for neuronal fate specification. Third, the primary (Bsh) and secondary (Ap) homeodomain TFs function in a feedforward loop to control the expression of synapse recognition molecule (DIP-β).

Homeodomain TFs are widely expressed across the nervous system in flies, worms, and mammals (Allen et al.; Davis et al., 2020; Reilly et al., 2020; Sugino et al., 2019; Zeisel et al., 2018). Thus, our findings may illuminate a conserved principle for how homeodomain TFs coordinately regulate neuronal fate and circuit assembly.

How can the single homeodomain TF Bsh specify two different neuron types: L4 and L5? We speculate that the Bsh might cooperate with Notch signaling to specify distinct neuron types. This is based on the well-characterized role of Notch in specifying binary cell fates during brain development (Bertet et al., 2014; Mark et al., 2021; Skeath and Doe, 1998; Spana and Doe, 1996; Truman et al., 2010), the role of Notch signaling specifying Ap+ sibling cell fate in the medulla neuroblast lineages (Li et al., 2013), and the fact that L4 is Ap+ and L5 is Ap-. An important future direction would be characterizing asymmetric distribution of Notch pathway components during L4 and L5 lamina neurogenesis, the role of Notch in specifying L4 and L5 neuronal fates, and whether/how Bsh and Notch are integrated to specify L4 and L5 neuron types.

Neurons express cell-type specific cell recognition molecules to recognize their correct synaptic partners and assemble into precise neural circuits. Our previous work showed DIP-β is specifically expressed in L4 neurons at the time of synapse formation and functions as synapse recognition molecule to regulate synaptic specificity (Xu et al., 2019). What are the genetic programs controlling the expression of DIP-β in L4 neurons at the time of synapse formation? Here we found that homeodomain TF Bsh activates another homeodomain TF Ap in L4 neurons, and then Bsh and Ap act together in a feedforward loop to drive DIP-β expression. Furthermore, we showed that Bsh binds directly to the *DIP-β* first intron in L4 neurons at the time of synapse formation. It would also be interesting to investigate whether Ap has direct binding site in the *DIP-β* first intron. Interestingly, a recent study found that EcR also has a DNA-binding motif in the *DIP-β* first intron and controls the temporal expression of *DIP-β* in L4 neurons (Jain et al., 2022). Together, we speculate that the homeodomain TF Bsh and the EcR pathway may cooperate to achieve the proper spatiotemporal expression pattern of the DIP-β synapse recognition molecule.

In addition, it is tempting to speculate about the evolutionary implications of our findings. Evolution drives a coordinated increase in neuronal diversity and functional complexity. An interesting open question is whether evolutionarily primitive insects, such as silverfish (Truman and Riddiford, 1999), lack Bsh expression and L4/L5 neuron orthologs, retaining only the core motion detection L1-L3 neurons. Our findings may provide a novel model whereby neural circuits evolve more complexity by adding the expression of a primary homeodomain TFs such as Bsh (Figure 7E).

**Acknowledgements**

We thank Stefan Abreo for technical assistance; Claude Desplan, Lawrence Zipursky, Makoto Sato, Markus Affolter, Richard Mann, Jing Peng, Cheng-Yu Lee, James Skeath, Cheng-Ting Chien for antibodies; Emily Nielson for the Fly Vision Box schematic; Claire Managan and Adam Taylor (Janelia Research Campus) for technical assistance and data processing; Lihi Zelnik-Manor and Pietro Perona (Caltech) for the original fly-tracking code; Project technical resources (Janelia Research Campus) for fig. S11 images; Ayanthi Bhattacharya and Sonia Sen for advice on the TaDa

experiment; and Claude Desplan, Vilaiwan Fernandes, Kristen Lee, Emily Heckman and Sarah Ackerman for comments on the manuscript. Stocks obtained from the Bloomington Drosophila Stock Center were used in this study.

## Author contributions

CX conceived of the project; performed and analyzed experiments, and generated initial drafts of the text and all figures; TBR performed and analyzed experiments; EMR generated fly lines for behavioral experiments; MBR designed and analyzed behavioral experiments; CQD provided feedback during the project, contributed to writing the paper and assembling the figures. All authors commented and approved of the manuscript.

## Declaration of interests

The authors declare no competing financial or non-financial interests.

# STAR METHODS

## Key resources table

| REAGENT or RESOURCE | SOURCE | IDENTIFIER |
|---|---|---|
| Antibodies | | |
| chicken anti-GFP (1:1000) | Abcam | Cat#ab13970, RRID_300798 |
| rabbit anti-Bsh (1:1000) | Gift from Claude Desplan (Özel et al., 2021) | N/A |
| guinea pig anti-Bsh (1:1000) | Gift from Lawrence Zipursky (Tan et al., 2015) & Makoto Soto (Hasegawa et al., 2011) | N/A |
| rabbit anti-Apterous (1:1000) | Gift from Markus Affolter (Bieli et al., 2015) | N/A |
| rat anti-Pdm3 (1:200) | Gift from Cheng-Ting Chien (Chen et al., 2012) | N/A |
| rabbit anti-Erm (1:100) | Gift from Cheng-Yu Lee (Janssens et al., 2014) | N/A |
| rat anti-Erm (1:70) | Gift from Jing Peng (Santiago et al., 2021) | N/A |
| mouse anti-Svp (1:10) | Developmental Studies Hybridoma Bank | Cat#Seven-up D2D3, RRID_2618079 |
| rat anti-Bab2 (1:20) | Gift from Claude Desplan & Lawrence Zipursky | N/A |
| rabbit anti-Zfh1 (1:1000) | Gift from James Skeath (Tian et al., 2004) | N/A |
| rabbit anti-Tailless (1:200) | Asian Distribution Center for Segmentation Antibodies | Code#812 |
| mouse anti-Dac (1:100) | Developmental Studies Hybridoma Bank | Cat#mAbdac1-1, RRID: AB_579773 |

| | | |
|---|---|---|
| mouse anti-Elav (1:200) | Developmental Studies Hybridoma Bank | Cat#Elav-9F8A9, RRID: AB_528217 |
| rat anti-Elav (1:50) | Developmental Studies Hybridoma Bank | Cat#Rat-Elav-7E8A10 anti-elav, RRID: AB_528218 |
| mouse anti-Chaoptin (1:20) | Developmental Studies Hybridoma Bank | Cat#24B10, RRID: AB_528161 |
| guinea pig anti-DIP- β (1:300) | Gift from Matthew Pecot Lab (Xu et al., 2019) | N/A |
| mouse anti-V5-TAG:Alexa Fluor® 647 (1:300) | Bio-Rad Laboratories | Cat#MCA1360A647, RRID: AB_770156 |
| rat anti-HA (1:100) | Sigma Aldrich | Cat#12158167001, RRID: AB_390915 |
| guinea pig anti-Hth (1:2000) | Gift from Richard Mann (Casares and Mann, 1998) | N/A |
| mouse anti-Brp (1:50) | Developmental Studies Hybridoma Bank | Cat#nc-82, RRID: AB_2314866 |
| Alexa Fluor 488 donkey anti-rat (1:400) | Jackson ImmunoResearch Lab | Cat#712-545-153, RRID: AB_2340684 |
| Alexa Fluor 488 donkey anti-chicken (1:400) | Jackson ImmunoResearch Lab | Cat#703-545-155, RRID: AB_2340375 |
| Alexa Fluor 488 donkey anti-guinea pig (1:400) | Jackson ImmunoResearch Lab | Cat#706-545-148, RRID: AB_2340472 |
| Alexa Fluor 488 donkey anti-rabbit (1:400) | Jackson ImmunoResearch Lab | Cat#711-545-152, RRID: AB_2313584 |
| Alexa Fluor 488 donkey anti-mouse (1:400) | Jackson ImmunoResearch Lab | Cat#715-545-150, RRID: AB_2340846 |
| Rhodamine Red-X donkey anti-mouse (1:400) | Jackson ImmunoResearch Lab | Cat#715-295-151, RRID: AB_2340832 |
| Rhodamine Red-X donkey anti-rat (1:400) | Jackson ImmunoResearch Lab | Cat#712-295-153, RRID: AB_2340676 |
| Rhodamine Red-X donkey anti-rabbit (1:400) | Jackson ImmunoResearch Lab | Cat#711-295-152, RRID: AB_2340613 |
| Rhodamine Red-X donkey anti-guinea pig (1:400) | Jackson ImmunoResearch Lab | Cat#706-295-148, RRID: AB_2340468 |
| Alexa Fluor 647 donkey anti-rabbit (1:400) | Jackson ImmunoResearch Lab | Cat#711-605-152, RRID: AB_2492288 |
| Alexa Fluor 647 donkey anti-mouse (1:400) | Jackson ImmunoResearch Lab | Cat#715-605-151, RRID: AB_2340863 |
| Alexa Fluor 647 donkey anti-guinea pig (1:400) | Jackson ImmunoResearch Lab | Cat#706-605-148, RRID: AB_2340476 |
| Alexa Fluor 647 donkey anti-rat (1:400) | Jackson ImmunoResearch Lab | Cat#712-605-153, RRID: AB_2340694 |
| Chemicals, peptides, and recombinant proteins | | |
| EDTA | Sigma-Aldrich | Cat#E6758 |
| QIAamp DNA Micro Kit | Qiagen | Cat#56304 |
| DpnI and CutSmart buffer | NEB | Cat#R0176S |
| PCR Purification Kit | Qiagen | Cat#28104 |
| DpnII and DpnII buffer | NEB | Cat#R0543S |
| MyTaq HS DNA Polymerase | Bioline | Cat#BIO-21112 |
| AlwI | NEB | Cat#R0513S |
| RNase A (DNase free) | Roche | Cat#11119915001 |
| T4 DNA ligase and 10x buffer | NEB | Cat#M0202S |

| Experimental models: Organisms/Strains | | |
|---|---|---|
| *D. melanogaster:* 10xUAS-IVS-myristoylated-GFP | Bloomington Drosophila Stock Center | RRID: BDSC_32198 |
| *D. melanogaster:* 27g05GAL4 | Bloomington Drosophila Stock Center | RRID: BDSC_48703 |
| *D. melanogaster:* UAS-Bsh-RNAi | Bloomington Drosophila Stock Center | RRID: BDSC_29336 |
| *D. melanogaster:* Bsh-LexA | Bloomington Drosophila Stock Center | RRID: BDSC_52834 |
| *D. melanogaster:* 13xLexAop-IVS-myr::GFP | Bloomington Drosophila Stock Center | RRID: BDSC_32211 |
| *D. melanogaster:* UAS-Cas9 | Bloomington Drosophila Stock Center | RRID: BDSC_58985 |
| *D. melanogaster:* UAS-Cas9 | Bloomington Drosophila Stock Center | RRID: BDSC_58986 |
| *D. melanogaster:* UAS-Bsh-sgRNA | Vienna Drosophila Resource Center | VDRC 341537 |
| *D. melanogaster:* UAS-ApRNAi | Bloomington Drosophila Stock Center | RRID: BDSC_41673 |
| *D. melanogaster:* 20xUAS-RSR.PEST | Bloomington Drosophila Stock Center | RRID: BDSC_55795 |
| *D. melanogaster:* UAS-Ap-shRNA | Vienna Drosophila Resource Center | VDRC 330463 |
| *D. melanogaster:* UAS-Bsh-HA | Bloomington Drosophila Stock Center | RRID: BDSC_83310 |
| *D. melanogaster:* tubP-GAL80[ts] | Bloomington Drosophila Stock Center | RRID: BDSC_7017 |
| *D. melanogaster:* UAS-Zfh1-RNAi | Vienna Drosophila Resource Center | VDRC 103205 |
| *D. melanogaster:* Brp-rst-stop-rst-smFPV5-2a-GAL4 | Jing Peng (Harvard Medical School) | N/A |
| *D. melanogaster:* 31C06AD (III), 34G07DBD (III) | Gift from Janelia Research Campus (Tuthill et al., 2013b) | N/A |
| *D. melanogaster:* 31C06-Gal4, UAS-myristoylated-tdTomato | Gift from Lawrence Zipursky | N/A |
| *D. melanogaster:* VALIUM20-mCherry | Bloomington Drosophila Stock Center | RRID: BDSC_35785 |
| *D. melanogaster:* Bsh-ORF-3XHA (86Fb) | FlyORF Webshop | Cat#F000054 |
| *D. melanogaster:* w; +/+; flyORF-TaDa | Gift from Owen Marshall Lab (Aughey et al., 2021) | RRID: BDSC_91637 |
| *D. melanogaster:* w; hs-FlpD5; FlyORF-TaDa | Gift from Owen Marshall Lab (Aughey et al., 2021) | RRID: BDSC_91638 |
| *D. melanogaster:* Bsh-TaDa | This paper | N/A |
| Oligonucleotides | | |
| DamID Adaptor (top strand): CTAATACGACTCACTATAGGGCAGCGTGGTCGCGGCCGAGGA | Integrated DNA technologies | N/A |
| DamID Adaptor (bottom strand): TCCTCGGCCG | Integrated DNA technologies | N/A |
| DamID Primer for PCR: GGTCGCGGCCGAGGATC | Integrated DNA technologies | N/A |
| Software and algorithms | | |
| Fiji | (Schindelin et al., 2012) | https://imagej.nih.gov/ij/download.html |
| MATlab | Mathworks | https://www.mathworks.com/products/matlab.html |

| | | |
|---|---|---|
| FastQC (v0.11.9) | The Babraham Bioinformatics group | https://www.bioinformatics.babraham.ac.uk/projects/download.html#fastqc |
| damidseq_pipeline | (Marshall and Brand, 2015) | https://owenjm.github.io/damidseq_pipeline/ |
| Bowtie2 (v2.4.5) | (Langmead and Salzberg, 2012) | http://bowtie-bio.sourceforge.net/bowtie2/index.shtml |
| IGV (v.2.13.2) | (Robinson et al., 2011) | https://software.broadinstitute.org/software/igv/download |
| SAMtools (v1.15.1) | (Li et al., 2009) | http://www.htslib.org/download/ |
| deepTools (v3.5.1) | (Ramírez et al., 2016) | https://deeptools.readthedocs.io/en/develop/content/installation.html |
| MACS2 (v2.2.7.1). | (Zhang et al., 2008) | https://pypi.org/project/MACS2/ |

## CONTACT FOR REAGENT AND RESOURCE SHARING

Further information and requests for resources and reagents should be directed to and will be fulfilled by the Lead Contact Chundi Xu (cxu3@uoregon.edu) and Chris Doe (cdoe@uoregon.edu).

## EXPERIMENTAL MODEL AND SUBJECT DETAILS

All flies were reared at 25°C on standard cornmeal fly food, unless otherwise stated. For all RNAi and shRNA knockdown experiments, crosses are kept at 25°C and their progeny are kept at 28.5°C with 16:8 hours light-dark cycle from the embryo stage until dissection.

## METHOD DETAILS

### Animal collections

For the Bsh-misexpression experiment, crosses were reared at 25°C in collection bottles fitted with 3.0% agar apple juice caps containing plain yeast paste. Embryos were then collected on 3.0% agar apple juice caps with plain yeast paste for 4 hours. The collected embryos were moved to 18°C until 72 hours after larval hatching (ALH). The larvae at 72h ALH were moved to 29°C until 58 hours after pupal formation.

For the experiment 27G05-GAL4>UAS-myrGFP, tubP-GAL80[ts], the progeny is kept in 18°C from embryo and moved to 29.2°C at early wandering L3 or 1d APF for 20 hours.

For the behavioral experiments, the progeny is kept in 18°C from embryo and moved to 29°C with 16:8 hours light-dark cycle from the early larval stage until behavioral tests. Male flies with 2-5days after the eclosion at 29°C were used for the Fly Vision Box experiments.

### Immunohistochemistry

Fly brains were dissected in Schneider's medium and fixed in 4% paraformaldehyde in phosphate buffered lysine for 25 min. After fixation, brains were quickly washed with phosphate buffer saline (PBS) with 0.5% Triton X-100 (PBT) and incubated in PBT for at least 2 hr at room temperature. Next, samples were incubated in blocking buffer (10% normal donkey serum, 0.5% Triton X-100 in

PBS) overnight at 4°C. Brains were then incubated in primary antibody (diluted in blocking buffer) at 4°C for at least two nights. Following primary antibody incubation, brains were washed with PBT. Next, brains were incubated in secondary antibody (diluted in blocking buffer) at 4°C for at least one day. Following secondary antibody incubation, brains were washed with PBT. Finally, brains were mounted in SlowFade Gold antifade reagent (Thermo Fisher Scientific, Waltham, MA).
Images were acquired using a Zeiss 800 confocal and processed with Image J and Adobe Photoshop.

**Knocking down homeodomain TF in neurons**

Genotype for knocking down Ap specifically in L4 neurons: 31C06-AD, 34G07-DBD>UAS-RSR, 79C23-S-GS-rst-stop-rst-smFPV5-2a-GAL4, UAS-Ap-shRNA. 31C06-AD, 34G07-DBD drives the expression of RSR recombinase in L4 neurons and RSR recombinase removes the "stop" code from 79C23-S-GS-rst-stop-rst-smFPV5-2a-GAL4. Therefore Brp-smFPV5-2a-GAL4 is transcribed and translated in L4 neurons into two proteins Brp-smFPV5 and GAL4. GAL4 together with 31C06-AD, 34G07-DBD drives the expression of Ap-shRNA to knockdown Ap. There is no Ap-KD efficiency when using 31C06-AD, 34G07-DBD to drive the expression of Ap-shRNA directly because 31C06-AD, 34G07-DBD depends on Ap expression.

**Generating Bsh-TaDa fly line**

Bsh-TaDa fly line was generated using the FlyORF-TaDa system described in (Aughey et al., 2021). Homozygous hs-FlpD5; FlyORF-TaDa virgin females were crossed to males from Bsh-ORF-3xHA line. Progeny (larval stage) were heat shocked at 37°C for 60 min, once per day. After eclosion, F1 male flies were crossed to MKRS/TM6B virgin females. F2 males and virgin females with the correct eye phenotype (w-; 3xP3-dsRed2+) were crossed to establish a balanced stock.

**TaDa in L4 neurons at the time of synapse formation**

Homozygous tubP-GAL80[ts]; 31C06-Gal4, UAS-myristoylated-tdTomato males were crossed to homozygous virgin females (FlyORF-TaDa line for Dam; Bsh-TaDa line for Bsh:Dam). Crosses were reared at 18°C. Pupas at 0h APF were staged at 18°C and then moved to 29.2°C after 3 days and 44 hours (age: 1d22h APF). After 24hours at 29.2°C, lamina (age: 3d4h APF) were collected in the cold PBS within one hour and stored at -20°C immediately until sufficient lamina were collected – for each group, about 70 lamina from 35 pupae. The TaDa experimental pipeline was followed according to (Marshall et al., 2016) with a few modifications. Briefly, DNA was extracted using a QIAamp DNA Micro Kit (Qiagen), digested with DpnI (NEB) overnight, and cleaned up using Qiagen PCR purification columns. DamID adaptors were ligated using T4 DNA ligase (NEB) followed by DpnII (NEB) digestion for 2 h and PCR amplification using MyTaq HS DNA polymerase (Bioline). The samples were sequenced on the NovaSeq at 118 base pairs and 27-33 million single end reads per sample.

**Bioinformatic analysis**

The TaDa sequencing data was analyzed as described previously (Sen et al., 2019). Briefly, each file was assessed for quality using FastQC (v0.11.9). The damidseq_pipeline was run to generate Log2 ratio bedgraph files (Bsh:Dam/Dam), Dam bam files and Bsh:Dam bam files as described previously (Marshall and Brand, 2015). The bedgraph files were used for data visualization on IGV (v.2.13.2) (Robinson et al., 2011). The read extended bam files were then used for peak calling using MACS2 (v2.2.7.1) (Zhang et al., 2008). For Bsh binding peaks in L4, narrow peaks were called on sorted, read extended Bsh:Dam bam file with Dam bam file as a control using the q-value cutoff of 0.001.

For L4 open chromatin, narrow peaks were called on sorted, read extended bam files of Dam without control using the q-value cutoff of 0.001. The bam files of Dam and Bsh:Dam were used to create sorted bam files and indexed bam files (bam.bai) using SAMtools (v1.15.1) (Li et al., 2009). Sorted bam files and indexed bam files were then computed using the multiBamSummary and plotCorrelation functions of deepTools (v3.5.1) (Ramírez et al., 2016) for correlation coefficients between biological replicates.
Binding sites for Bsh (M1089) across the genome were identified using PWMscan (https://ccg.epfl.ch/pwmtools/pwmscan) (Ambrosini et al., 2018) with the p-value cutoff of 0.00001.

**Behavioral experiments**

The Fly Vision Box apparatus was developed at the Janelia Research Campus as a high-throughput assay integrating several tests of visually guided behavior for flies in tubes. Groups of flies (usually 10-15) are placed in the clear acrylic tubes, inside a temperature-controlled box. The box contains 6 tubes, each with a strip of green LEDs (patterns of 4 pixels on / 4 pixels off moving at the indicated temporal frequency or contrast) lining one wall, for the motion vision experiments, and a single green and single UV LED on each end of each corridor, for the phototaxis and spectral-preference assays. During the spectral preference task, a green LED is illuminated (at level 10) at the end of each tube, while at the opposite end of the tubes a UV LED is illuminated at increasing brightness levels. The tubes are capped with a polished acrylic plug that is transparent. 4 small (pager) motors are mounted on the corners of the box to provide a mechanical startle in between trials. A camera mounted above the box records fly movements at 25 frames/s. The camera is fitted with an Infrared-passing filter and the tubes are suspended above an Infrared backlight.

In visual motion response assay, stimulus with different temporal frequency (0, 0.5, 2, 5, 10, 20, 42 HZ) or 5Hz temporal frequency, but with the indicated contrast level were given. The flies walk against the direction of motion, quantified with a Direction Index. The phototaxis behavior measures the movement of flies towards UV or green LED with the indicated (relative) intensity level at the end of the tubes. The Direction Index is shown integrated over each trial length. In spectral preference task, for lower UV levels, flies walk towards the green LED, but walk towards the UV LED at higher UV levels.

A full experiment lasts ~30 minutes and consists of 44 conditions, presented in short blocks, during which a series of conditions (e.g. the 4 LED settings for the phototaxis assay) are presented twice (for Phototaxis) or 4 times each for the other tests, where on consecutive trials the stimulus is presented with opposite direction (for motion) or at the opposite ends of the tubes (for phototaxis and spectral preference). Each trial begins immediately after a 0.5 s mechanical startle by the motors. The box is heated to 34°C. The heating and motorized startle ensure that flies are active throughout and respond to these stimuli.

**Quantification and Statistical Analysis for behavioral experiments**

Videos are tracked offline with custom code written in MATLAB. After tracking, the trajectories were analyzed on a per-frame basis to see whether flies were walking in one direction (either following the moving patterns or walking towards one end-cap LED) or the other. The behavior is summarized as a 'Direction Index' which is simply the difference between flies walking in one direction and the other (by convention the direction against the motion, or towards the illuminated LED, is the positive one) divided by the total number of flies in the tube. For example, with 12 flies

in a tube, during one frame, 7 are moving in the positive direction and 4 are moving in the negative direction (and 1 is not moving), then for this frame, DI = (7-4)/12 = 0.25.

For the summarized plots in Figure 7, the Direction Index is averaged over the entire 10 second duration of each motion stimulus trial. For the phototaxis and spectral preference experiments, the DI is integrated (accumulated) across time and the data recorded for each trial is the peak (negative or positive) of this curve. For the 10 or 15 second trials, the maximum possible value is 10 or 15 (10, 15 s × 1). Individual data points in Figure 7 represent the mean or peak DI metric summarizing all the flies in each tube, and the summary data are the mean and standard deviation across tubes.

The data summarized are part of a larger series of experimental conditions that include several other tasks that are largely redundant with those presented. Nevertheless, the flies experienced 44 different conditions, and so all data were used for a False Discovery Rate controlling procedure (Benjamini and Hochberg, 1995)with q = 0.05. The data from conditions not shown do not contain additional tests with statistically significant differences between the 2 tested genotypes.

**Quantification of DIP-β fluorescence signal**

Using image J, we quantified DIP-β signal in control and knockdown brains by measuring fluorescence signal along the long axis of lamina cartridges (see white lines in Figure 5A) from the distal dash line to the proximal dash line (3 cartridges per brain). Signal intensity values and cartridge lengths were converted to percentages by setting the highest intensity within each cartridge as 100% intensity and the full length of the cartridge as 100% distance. Statistical analysis using unpaired t tests was performed after setting uniform intervals (using the spline function on MATLAB) of 0.01% distance. We presented 20-100% as 0-100% to focus on L4 signal (the first 20% is DIP- β signal in LaWF2).

**Quantification of Brp puncta in the distal and proximal regions of lamina cartridges**

Using confocal microscopy, we generated z-stacks of the lamina down the long axis of lamina cartridges. Within each z-stack (i.e. each optic lobe) 20 cartridges in the center of the lamina were identified and the number of Brp puncta in their distal halves was counted. The top (distal edge; top dash line in Figure 5E) and bottom (proximal edge; bottom dash line in Figure 5E)) of each cartridge was determined by the first section below L4 cell body and last section containing L4 neuron processes (myrtd::TOM), respectively. The midpoint of each cartridge was then identified as the section in between the top and bottom sections. Brp puncta were counted in the sections distal to the midpoint of each cartridge as distal Brp puncta and in the sections proximal to the midpoint of each cartridge as proximal Brp puncta. Genotypes were scored in a blind manner.

**Quantification of L4 proximal neurite length**

In the same cartridges as those chosen to quantify the Brp puncta, the number of z-stacks that contained L4 proximal neurites were calculated as a percentage of the entire long axis, and represented the values presented for proximal neurite length.

**Statistical Analysis**

Statistics were performed using a combination of Microsoft Excel, MATLAB (MathWorks) and Prism (GraphPad) software. Unpaired t-test was used, unless otherwise noted. Data are presented as mean ± SEM unless otherwise noted. A 95% confidence interval was used to define the level of

472 significance. * $P < 0.05$, ** $P < 0.01$, *** $P < 0.001$, ns=not significant. All other relevant statistical
473 information can be found in the figure legends.
474
475

## References


Allen, A.M., Neville, M.C., Birtles, S., Croset, V., Treiber, C.D., Waddell, S., and Goodwin, S.F. A single-cell transcriptomic atlas of the adult Drosophila ventral nerve cord. ELife *9*, e54074. https://doi.org/10.7554/eLife.54074.

Ambrosini, G., Groux, R., and Bucher, P. (2018). PWMScan: a fast tool for scanning entire genomes with a position-specific weight matrix. Bioinformatics *34*, 2483–2484. https://doi.org/10.1093/bioinformatics/bty127.

Aughey, G.N., Delandre, C., McMullen, J.P.D., Southall, T.D., and Marshall, O.J. (2021). FlyORF-TaDa allows rapid generation of new lines for in vivo cell-type-specific profiling of protein–DNA interactions in Drosophila melanogaster. G3 GenesGenomesGenetics *11*, jkaa005. https://doi.org/10.1093/g3journal/jkaa005.

Bayraktar, O.A., and Doe, C.Q. (2013). Combinatorial temporal patterning in progenitors expands neural diversity. Nature *498*, 449–455. https://doi.org/10.1038/nature12266.

Benjamini, Y., and Hochberg, Y. (1995). Controlling the False Discovery Rate: A Practical and Powerful Approach to Multiple Testing. J. R. Stat. Soc. Ser. B Methodol. *57*, 289–300. https://doi.org/10.1111/j.2517-6161.1995.tb02031.x.

Benzer, S. (1967). BEHAVIORAL MUTANTS OF Drosophila ISOLATED BY COUNTERCURRENT DISTRIBUTION. Proc. Natl. Acad. Sci. *58*, 1112–1119. https://doi.org/10.1073/pnas.58.3.1112.

Bertet, C., Li, X., Erclik, T., Cavey, M., Wells, B., and Desplan, C. (2014). Temporal patterning of neuroblasts controls Notch-mediated cell survival through regulation of Hid or Reaper. Cell *158*, 1173–1186. https://doi.org/10.1016/j.cell.2014.07.045.

Briscoe, J., Pierani, A., Jessell, T.M., and Ericson, J. (2000). A Homeodomain Protein Code Specifies Progenitor Cell Identity and Neuronal Fate in the Ventral Neural Tube. Cell *101*, 435–445. https://doi.org/10.1016/S0092-8674(00)80853-3.

Casares, F., and Mann, R.S. (1998). Control of antennal versus leg development in Drosophila. Nature *392*, 723–726. https://doi.org/10.1038/33706.

Chen, C.-K., Chen, W.-Y., and Chien, C.-T. (2012). The POU-domain protein Pdm3 regulates axonal targeting of R neurons in the Drosophila ellipsoid body. Dev. Neurobiol. *72*, 1422–1432. https://doi.org/10.1002/dneu.22003.

Chen, Y., Akin, O., Nern, A., Tsui, C.Y.K., Pecot, M.Y., and Zipursky, S.L. (2014). Cell-type-Specific Labeling of Synapses In Vivo through Synaptic Tagging with Recombination. Neuron *81*, 280–293. https://doi.org/10.1016/j.neuron.2013.12.021.

Cubelos, B., Sebastián-Serrano, A., Beccari, L., Calcagnotto, M.E., Cisneros, E., Kim, S., Dopazo, A., Alvarez-Dolado, M., Redondo, J.M., Bovolenta, P., et al. (2010). Cux1 and Cux2 Regulate

Dendritic Branching, Spine Morphology, and Synapses of the Upper Layer Neurons of the Cortex. Neuron *66*, 523–535. https://doi.org/10.1016/j.neuron.2010.04.038.

Davis, F.P., Nern, A., Picard, S., Reiser, M.B., Rubin, G.M., Eddy, S.R., and Henry, G.L. (2020). A genetic, genomic, and computational resource for exploring neural circuit function. ELife *9*, e50901. https://doi.org/10.7554/eLife.50901.

De Marco Garcia, N.V., and Jessell, T.M. (2008). Early Motor Neuron Pool Identity and Muscle Nerve Trajectory Defined by Postmitotic Restrictions in Nkx6.1 Activity. Neuron *57*, 217–231. https://doi.org/10.1016/j.neuron.2007.11.033.

Deneris, E.S., and Hobert, O. (2014). Maintenance of postmitotic neuronal cell identity. Nat. Neurosci. *17*, 899–907. https://doi.org/10.1038/nn.3731.

Doe, C.Q. (2017). Temporal Patterning in the Drosophila CNS. Annu. Rev. Cell Dev. Biol. *33*, 219–240. https://doi.org/10.1146/annurev-cellbio-111315-125210.

Enriquez, J., Venkatasubramanian, L., Baek, M., Peterson, M., Aghayeva, U., and Mann, R.S. (2015). Specification of Individual Adult Motor Neuron Morphologies by Combinatorial Transcription Factor Codes. Neuron *86*, 955–970. https://doi.org/10.1016/j.neuron.2015.04.011.

Erclik, T., Li, X., Courgeon, M., Bertet, C., Chen, Z., Baumert, R., Ng, J., Koo, C., Arain, U., Behnia, R., et al. (2017). Integration of temporal and spatial patterning generates neural diversity. Nature *541*, 365–370. https://doi.org/10.1038/nature20794.

Ericson, J., Rashbass, P., Schedl, A., Brenner-Morton, S., Kawakami, A., van Heyningen, V., Jessell, T.M., and Briscoe, J. (1997). Pax6 Controls Progenitor Cell Identity and Neuronal Fate in Response to Graded Shh Signaling. Cell *90*, 169–180. https://doi.org/10.1016/S0092-8674(00)80323-2.

Gao, S., Takemura, S., Ting, C.-Y., Huang, S., Lu, Z., Luan, H., Rister, J., Thum, A.S., Yang, M., Hong, S.-T., et al. (2008). The Neural Substrate of Spectral Preference in Drosophila. Neuron *60*, 328–342. https://doi.org/10.1016/j.neuron.2008.08.010.

Hasegawa, E., Kaido, M., Takayama, R., and Sato, M. (2013). Brain-specific-homeobox is required for the specification of neuronal types in the Drosophila optic lobe. Dev. Biol. *377*, 90–99. https://doi.org/10.1016/j.ydbio.2013.02.012.

Hobert, O. (2021). Homeobox genes and the specification of neuronal identity. Nat. Rev. Neurosci. *22*, 627–636. https://doi.org/10.1038/s41583-021-00497-x.

Hobert, O., and Kratsios, P. (2019). Neuronal identity control by terminal selectors in worms, flies, and chordates. Curr. Opin. Neurobiol. *56*, 97–105. https://doi.org/10.1016/j.conb.2018.12.006.

Holguera, I., and Desplan, C. (2018). Neuronal specification in space and time. Science *362*, 176–180. https://doi.org/10.1126/science.aas9435.

545 Jain, S., Lin, Y., Kurmangaliyev, Y.Z., Valdes-Aleman, J., LoCascio, S.A., Mirshahidi, P.,
546 Parrington, B., and Zipursky, S.L. (2022). A global timing mechanism regulates cell-type-specific
547 wiring programmes. Nature *603*, 112–118. https://doi.org/10.1038/s41586-022-04418-5.

548 Janssens, D.H., Komori, H., Grbac, D., Chen, K., Koe, C.T., Wang, H., and Lee, C.-Y. (2014).
549 Earmuff restricts progenitor cell potential by attenuating the competence to respond to self-renewal
550 factors. Dev. Camb. Engl. *141*, 1036–1046. https://doi.org/10.1242/dev.106534.

551 Langmead, B., and Salzberg, S.L. (2012). Fast gapped-read alignment with Bowtie 2. Nat. Methods
552 *9*, 357–359. https://doi.org/10.1038/nmeth.1923.

553 Leyva-Díaz, E., and Hobert, O. (2019). Transcription factor autoregulation is required for acquisition
554 and maintenance of neuronal identity. Development *146*, dev177378.
555 https://doi.org/10.1242/dev.177378.

556 Li, H., Handsaker, B., Wysoker, A., Fennell, T., Ruan, J., Homer, N., Marth, G., Abecasis, G.,
557 Durbin, R., and 1000 Genome Project Data Processing Subgroup (2009). The Sequence
558 Alignment/Map format and SAMtools. Bioinforma. Oxf. Engl. *25*, 2078–2079.
559 https://doi.org/10.1093/bioinformatics/btp352.

560 Li, X., Erclik, T., Bertet, C., Chen, Z., Voutev, R., Venkatesh, S., Morante, J., Celik, A., and
561 Desplan, C. (2013). Temporal patterning of Drosophila medulla neuroblasts controls neural fates.
562 Nature *498*, 456–462. https://doi.org/10.1038/nature12319.

563 Mark, B., Lai, S.-L., Zarin, A.A., Manning, L., Pollington, H.Q., Litwin-Kumar, A., Cardona, A.,
564 Truman, J.W., and Doe, C.Q. (2021). A developmental framework linking neurogenesis and circuit
565 formation in the Drosophila CNS. ELife *10*. https://doi.org/10.7554/eLife.67510.

566 Marshall, O.J., and Brand, A.H. (2015). damidseq_pipeline: an automated pipeline for processing
567 DamID sequencing datasets. Bioinformatics *31*, 3371–3373.
568 https://doi.org/10.1093/bioinformatics/btv386.

569 Marshall, O.J., Southall, T.D., Cheetham, S.W., and Brand, A.H. (2016). Cell-type-specific profiling
570 of protein-DNA interactions without cell isolation using targeted DamID with next-generation
571 sequencing. Nat. Protoc. *11*, 1586–1598. https://doi.org/10.1038/nprot.2016.084.

572 Meinertzhagen, I.A., and O'Neil, S.D. (1991). Synaptic organization of columnar elements in the
573 lamina of the wild type in Drosophila melanogaster. J. Comp. Neurol. *305*, 232–263.
574 https://doi.org/10.1002/cne.903050206.

575 Pereira, L., Kratsios, P., Serrano-Saiz, E., Sheftel, H., Mayo, A.E., Hall, D.H., White, J.G., LeBoeuf,
576 B., Garcia, L.R., Alon, U., et al. (2015). A cellular and regulatory map of the cholinergic nervous
577 system of C. elegans. ELife *4*, e12432. https://doi.org/10.7554/eLife.12432.

578 Piñeiro, C., Lopes, C.S., and Casares, F. (2014). A conserved transcriptional network regulates
579 lamina development in the Drosophila visual system. Dev. Camb. *141*, 2838–2847.
580 https://doi.org/10.1242/dev.108670.

Ramírez, F., Ryan, D.P., Grüning, B., Bhardwaj, V., Kilpert, F., Richter, A.S., Heyne, S., Dündar, F., and Manke, T. (2016). deepTools2: a next generation web server for deep-sequencing data analysis. Nucleic Acids Res. *44*, W160–W165. https://doi.org/10.1093/nar/gkw257.

Reilly, M.B., Cros, C., Varol, E., Yemini, E., and Hobert, O. (2020). Unique homeobox codes delineate all the neuron classes of C. elegans. Nature *584*, 595–601. https://doi.org/10.1038/s41586-020-2618-9.

Rivera-Alba, M., Vitaladevuni, S.N., Mishchenko, Y., Lu, Z., Takemura, S., Scheffer, L., Meinertzhagen, I.A., Chklovskii, D.B., and de Polavieja, G.G. (2011). Wiring Economy and Volume Exclusion Determine Neuronal Placement in the Drosophila Brain. Curr. Biol. *21*, 2000–2005. https://doi.org/10.1016/j.cub.2011.10.022.

Robinson, J.T., Thorvaldsdóttir, H., Winckler, W., Guttman, M., Lander, E.S., Getz, G., and Mesirov, J.P. (2011). Integrative genomics viewer. Nat. Biotechnol. *29*, 24–26. https://doi.org/10.1038/nbt.1754.

Santiago, I.J., Zhang, D., Saras, A., Pontillo, N., Xu, C., Chen, X., Weirauch, M.T., Mistry, M., Ginty, D.D., Pecot, M.Y., et al. (2021). Drosophila Fezf functions as a transcriptional repressor to direct layer-specific synaptic connectivity in the fly visual system. Proc. Natl. Acad. Sci. *118*. https://doi.org/10.1073/pnas.2025530118.

Schindelin, J., Arganda-Carreras, I., Frise, E., Kaynig, V., Longair, M., Pietzsch, T., Preibisch, S., Rueden, C., Saalfeld, S., Schmid, B., et al. (2012). Fiji: an open-source platform for biological-image analysis. Nat. Methods *9*, 676–682. https://doi.org/10.1038/nmeth.2019.

Sen, S.Q., Chanchani, S., Southall, T.D., and Doe, C.Q. (2019). Neuroblast-specific open chromatin allows the temporal transcription factor, Hunchback, to bind neuroblast-specific loci. ELife *8*, e44036. https://doi.org/10.7554/eLife.44036.

Serrano-Saiz, E., Leyva-Díaz, E., De La Cruz, E., and Hobert, O. (2018). BRN3-type POU Homeobox Genes Maintain the Identity of Mature Postmitotic Neurons in Nematodes and Mice. Curr. Biol. *28*, 2813-2823.e2. https://doi.org/10.1016/j.cub.2018.06.045.

Silies, M., Gohl, D.M., Fisher, Y.E., Freifeld, L., Clark, D.A., and Clandinin, T.R. (2013). Modular Use of Peripheral Input Channels Tunes Motion-Detecting Circuitry. Neuron *79*, 111–127. https://doi.org/10.1016/j.neuron.2013.04.029.

Skeath, J.B., and Doe, C.Q. (1998). Sanpodo and Notch act in opposition to Numb to distinguish sibling neuron fates in the Drosophila CNS. Development *125*, 1857–1865. .

Spana, E.P., and Doe, C.Q. (1996). Numb Antagonizes Notch Signaling to Specify Sibling Neuron Cell Fates. Neuron *17*, 21–26. https://doi.org/10.1016/S0896-6273(00)80277-9.

Sugino, K., Clark, E., Schulmann, A., Shima, Y., Wang, L., Hunt, D.L., Hooks, B.M., Tränkner, D., Chandrashekar, J., Picard, S., et al. (2019). Mapping the transcriptional diversity of genetically and anatomically defined cell populations in the mouse brain. ELife *8*, e38619. https://doi.org/10.7554/eLife.38619.

Takemura, S., Xu, C.S., Lu, Z., Rivlin, P.K., Parag, T., Olbris, D.J., Plaza, S., Zhao, T., Katz, W.T., Umayam, L., et al. (2015). Synaptic circuits and their variations within different columns in the visual system of *Drosophila*. Proc. Natl. Acad. Sci. *112*, 13711–13716. https://doi.org/10.1073/pnas.1509820112.

Tan, L., Zhang, K.X., Pecot, M.Y., Nagarkar-Jaiswal, S., Lee, P.-T., Takemura, S., McEwen, J.M., Nern, A., Xu, S., Tadros, W., et al. (2015). Ig Superfamily Ligand and Receptor Pairs Expressed in Synaptic Partners in Drosophila. Cell *163*, 1756–1769. https://doi.org/10.1016/j.cell.2015.11.021.

Thor, S., and Thomas, J.B. (1997). The Drosophila islet Gene Governs Axon Pathfinding and Neurotransmitter Identity. Neuron *18*, 397–409. https://doi.org/10.1016/S0896-6273(00)81241-6.

Tian, X., Hansen, D., Schedl, T., and Skeath, J.B. (2004). Epsin potentiates Notch pathway activity in Drosophila and C. elegans. Dev. Camb. Engl. *131*, 5807–5815. https://doi.org/10.1242/dev.01459.

Truman, J.W., and Riddiford, L.M. (1999). The origins of insect metamorphosis. Nature *401*, 447–452. https://doi.org/10.1038/46737.

Truman, J.W., Moats, W., Altman, J., Marin, E.C., and Williams, D.W. (2010). Role of Notch signaling in establishing the hemilineages of secondary neurons in Drosophila melanogaster. Development *137*, 53–61. https://doi.org/10.1242/dev.041749.

Tuthill, J.C., Nern, A., Holtz, S.L., Rubin, G.M., and Reiser, M.B. (2013). Contributions of the 12 Neuron Classes in the Fly Lamina to Motion Vision. Neuron *79*, 128–140. https://doi.org/10.1016/j.neuron.2013.05.024.

Xu, C., Theisen, E., Maloney, R., Peng, J., Santiago, I., Yapp, C., Werkhoven, Z., Rumbaut, E., Shum, B., Tarnogorska, D., et al. (2019). Control of Synaptic Specificity by Establishing a Relative Preference for Synaptic Partners. Neuron *103*, 865-877.e7. https://doi.org/10.1016/j.neuron.2019.06.006.

Zeisel, A., Hochgerner, H., Lönnerberg, P., Johnsson, A., Memic, F., van der Zwan, J., Häring, M., Braun, E., Borm, L.E., La Manno, G., et al. (2018). Molecular Architecture of the Mouse Nervous System. Cell *174*, 999-1014.e22. https://doi.org/10.1016/j.cell.2018.06.021.

Zhang, Y., Liu, T., Meyer, C.A., Eeckhoute, J., Johnson, D.S., Bernstein, B.E., Nusbaum, C., Myers, R.M., Brown, M., Li, W., et al. (2008). Model-based Analysis of ChIP-Seq (MACS). Genome Biol. *9*, R137. https://doi.org/10.1186/gb-2008-9-9-r137.

Zhu, Y., Nern, A., Zipursky, S.L., and Frye, M.A. (2009). Peripheral Visual Circuits Functionally Segregate Motion and Phototaxis Behaviors in the Fly. Curr. Biol. *19*, 613–619. https://doi.org/10.1016/j.cub.2009.02.053.

Fig. 1

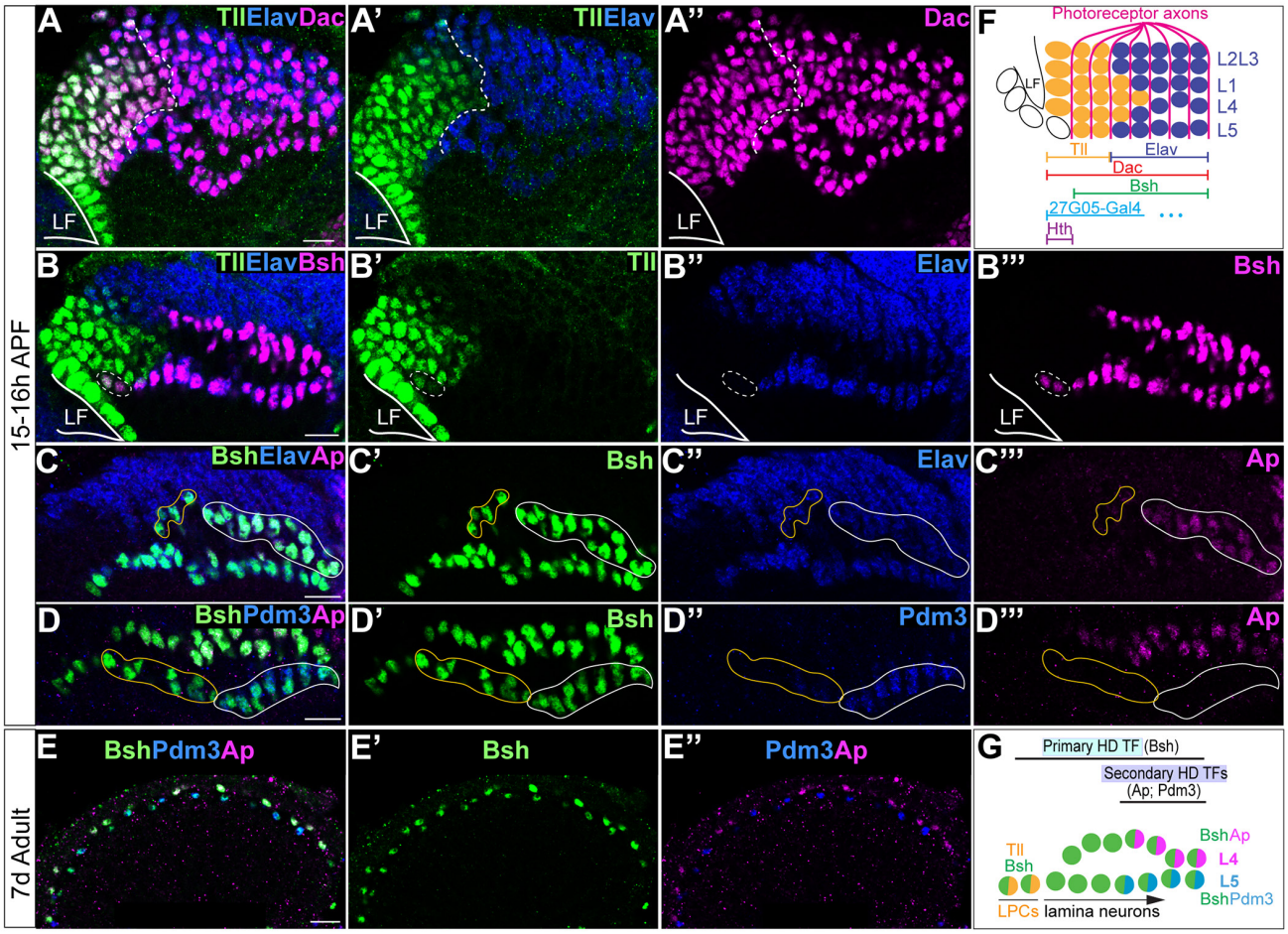


**Figure 1. Sequential initiation of homeodomain TFs during lamina neurogenesis**

(A-A'') Tll is identified as an LPC marker, expressed complementary to Elav; Dac labels both Tll+ LPCs and Elav+ neurons. LF: lamina furrow. Here and below, scale bar: 10 µm, n≥5 brains.

(B-B''') Bsh is expressed in Tll+ Elav- LPCs (white dash circle) and maintained in Elav+ L4 and L5 neurons.

(C-C''') Ap is expressed in L4 neurons. Newborn L4 neurons are Bsh+ Elav+ Ap- (yellow line circle), while older L4 neurons are Bsh+ Elav+ Ap+ (white line circle).

(D-D''') Pdm3 is expressed in L5 neurons. Newborn L5 neurons are Bsh+ Pdm3- (yellow line circle), while older L5 neurons are Bsh+ Pdm3+ (white line circle).

(E-E'') Bsh, Ap and Pdm3 expressions are maintained in adult.

(F) Schematic of lamina neuron development in early pupa.

(G) Summary.

See also Figures S1A-S1A'''.

Fig. 2

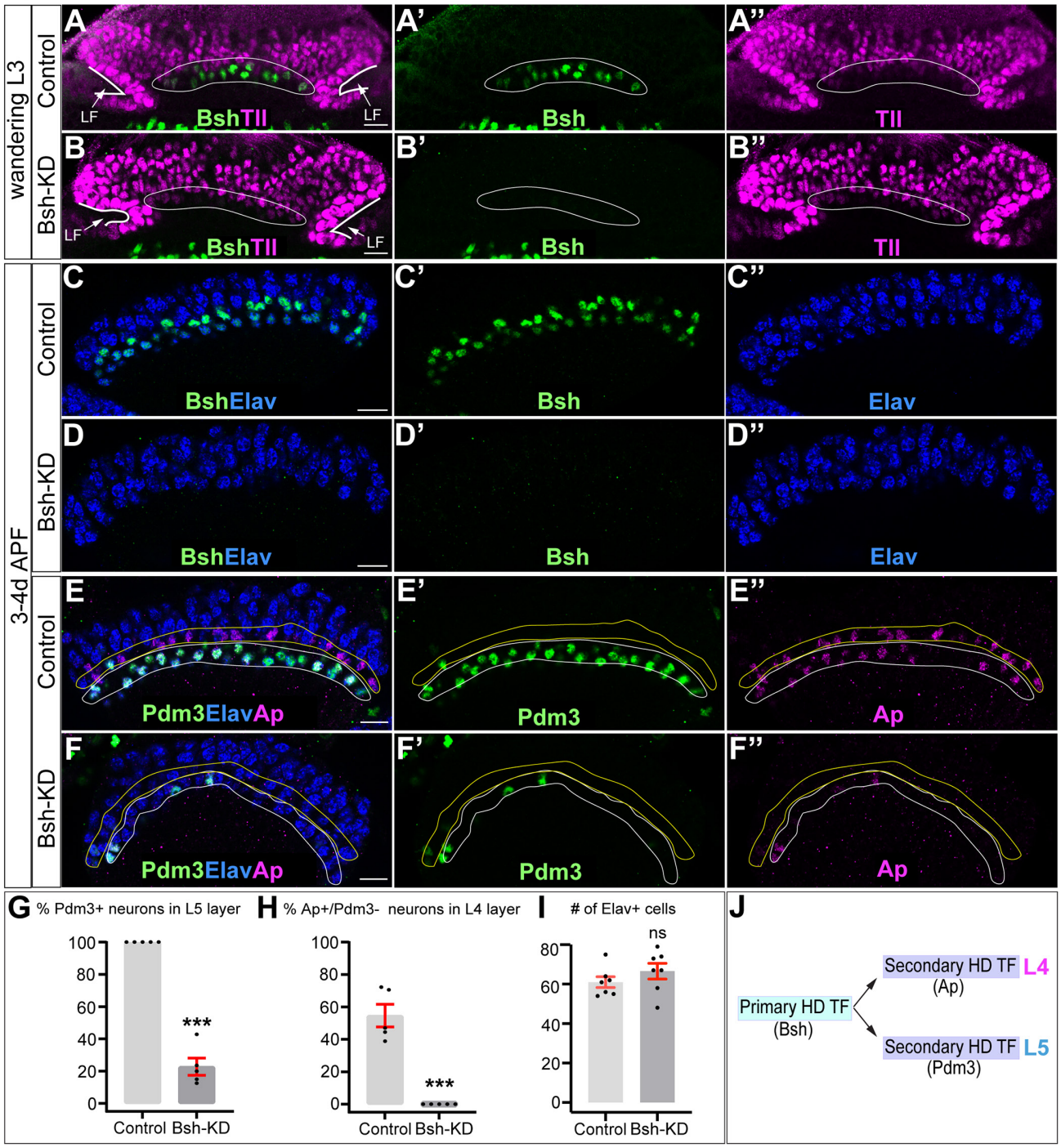


**Figure 2. Bsh activates Ap/Pdm3 expression and specifies L4/L5 neuronal fate**

(A-B'') Bsh-KD in LPCs (27G05-Gal4>UAS-Bsh-RNAi) eliminates Bsh in LPCs and neurons in wandering L3 (white circle). Tll labels all LPCs. LF: lamina furrow. L3: third larval instar. Here and below, scale bar: 10 µm, n≥5 brains.

(C-D'') Bsh remains undetectable in the lamina of 3-4day pupa in Bsh-KD (27G05-Gal4>UAS-Bsh-RNAi).

679 (E-I) Bsh-KD in LPCs removes most L4 (Bsh/Ap) (H) and L5 (Bsh/Pdm3) (G) neuron markers. The
680 Ap expression in L5 is caused by the Gal4 driver line but is irrelevant here. (I) The number of Elav+
681 cells in single slice. n=5 brains in (G) and (H), n=7 brains in (I). ***$P$<0.001, ns=not significant,
682 unpaired t-test, each dot represents each brain, data are presented as mean ± SEM. L4 layer, yellow
683 outline. L5 layer, white outline.
684 See also Figures S1B-S1F and S2-S4.

Fig. 3

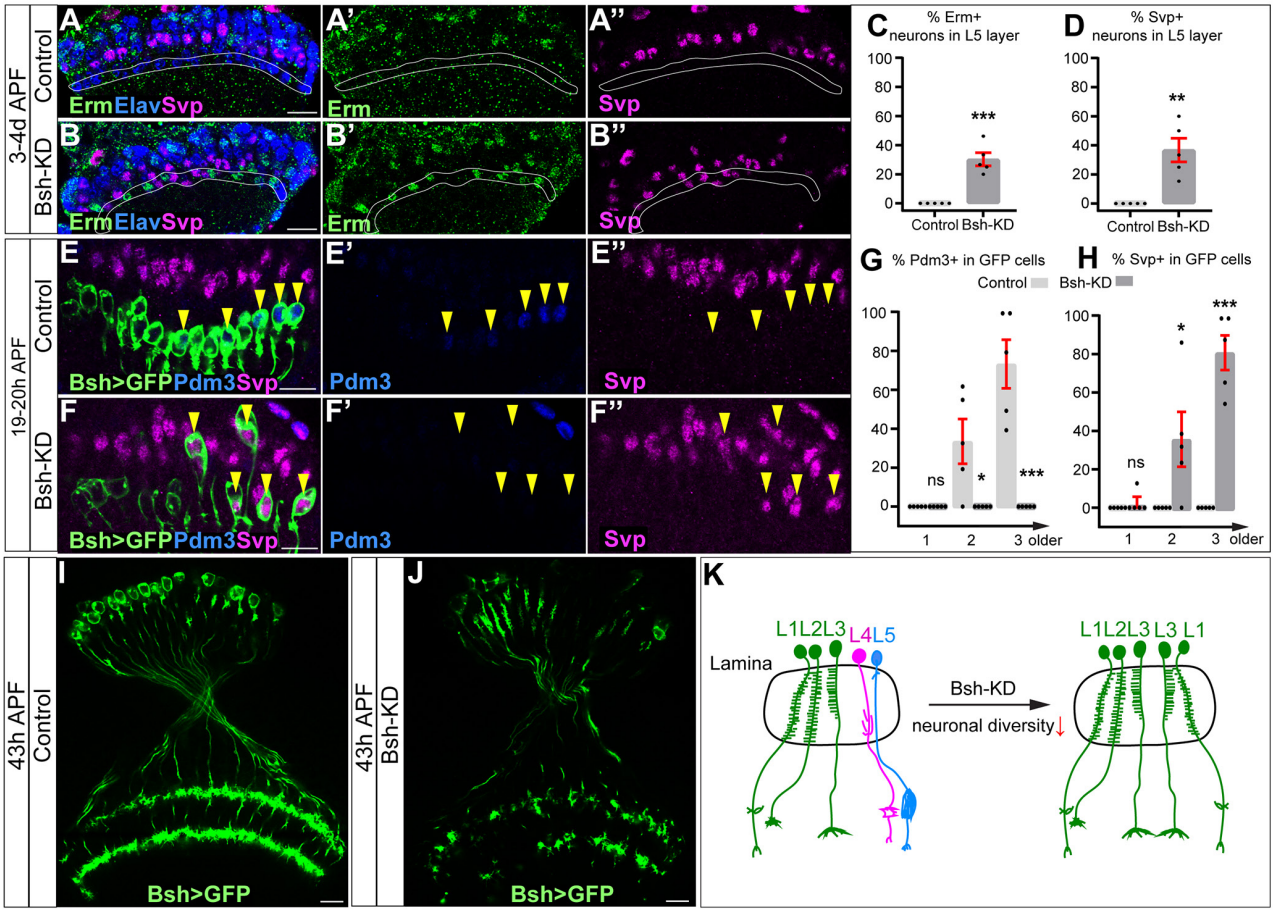


**Figure 3. Bsh suppresses L1/L3 neuronal fate**

(A-D) Bsh-KD in LPCs results in the ectopic expression of the L1 marker Svp (D) and L3 marker Erm (C) in L4/L5 cell body layers.

(E-H) Bsh-KD in LPCs results in ectopic Svp+ L1 neurons (H) at the expense of Pdm3+ L5 neurons (G) (Bsh-LexA>LexAop-GFP). Bsh:GFP+ neurons marked with yellow arrowheads show L1 marker Svp expression in Bsh-KD while L5 marker Pdm3 expression in control.

(I and J) Ectopic Svp+ L1 neurons at the expense of L5 neurons in Bsh-KD adopt L1-like morphology (Bsh-LexA>LexAop-GFP).

(K) Summary.

Data are presented as mean ± SEM. Each dot represents each brain. n=5 brains in (C), (D), (G), and (H). *$P$<0.05, **$P$<0.01, ***$P$<0.001, ns=not significant, unpaired t-test.

See also Figures S5-S7.

Fig. 4

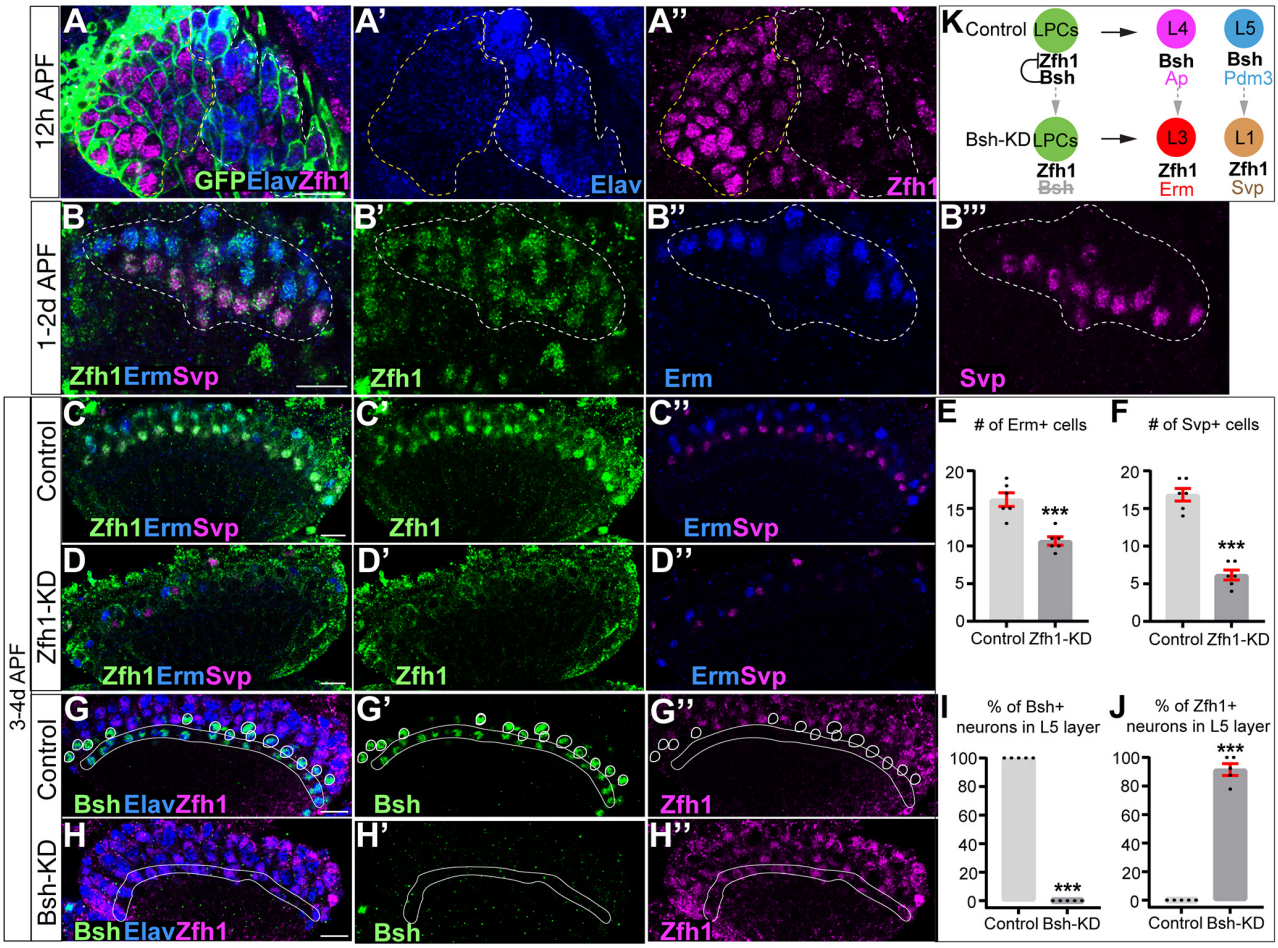


**Figure 4. Bsh represses Zfh1 to suppress L1/L3 neuronal fate**

(A-A'') Zfh1 is expressed in all LPCs and some lamina neurons at 12h APF. GFP (27G05-Gal4>UAS-myrGFP) labels all lamina cells. Elav labels lamina neurons. Yellow dash circle outlines LPCs and white dash circle outlines lamina neurons. Here and below, scale bar, 10 µm. n≥5 brains.

(B- B''') Zfh1 is expressed in L1 (Svp+) and L3 neurons (Erm+) at 1-2d APF. White dash circle outlines L1 and L3 neurons.

(C-F) Zfh1-KD in LPCs results in a loss of Svp+ L1 and Erm+ L3 neurons. (E and F) The number of Erm+ (E) or Svp+ (F) cell bodies in single slice in control (C) and Zfh1-KD (D).

(G to J) Bsh-KD in LPCs results in ectopic Zfh1 in L4/L5 layers. White circles label Bsh+ cell bodies in L4 layer in control. L5 layer, white outline. (I and J) The percentage of Bsh+ (I) or Zfh1+ (J) neurons in L5 layer.

(K) Summary.

Data are presented as mean ± SEM. Each dot represents each brain. n=6 brains in (E), (F), (I) and (J). ***$P$<0.001, unpaired t-test.

See also Figures S5E and S8.

Fig. 5

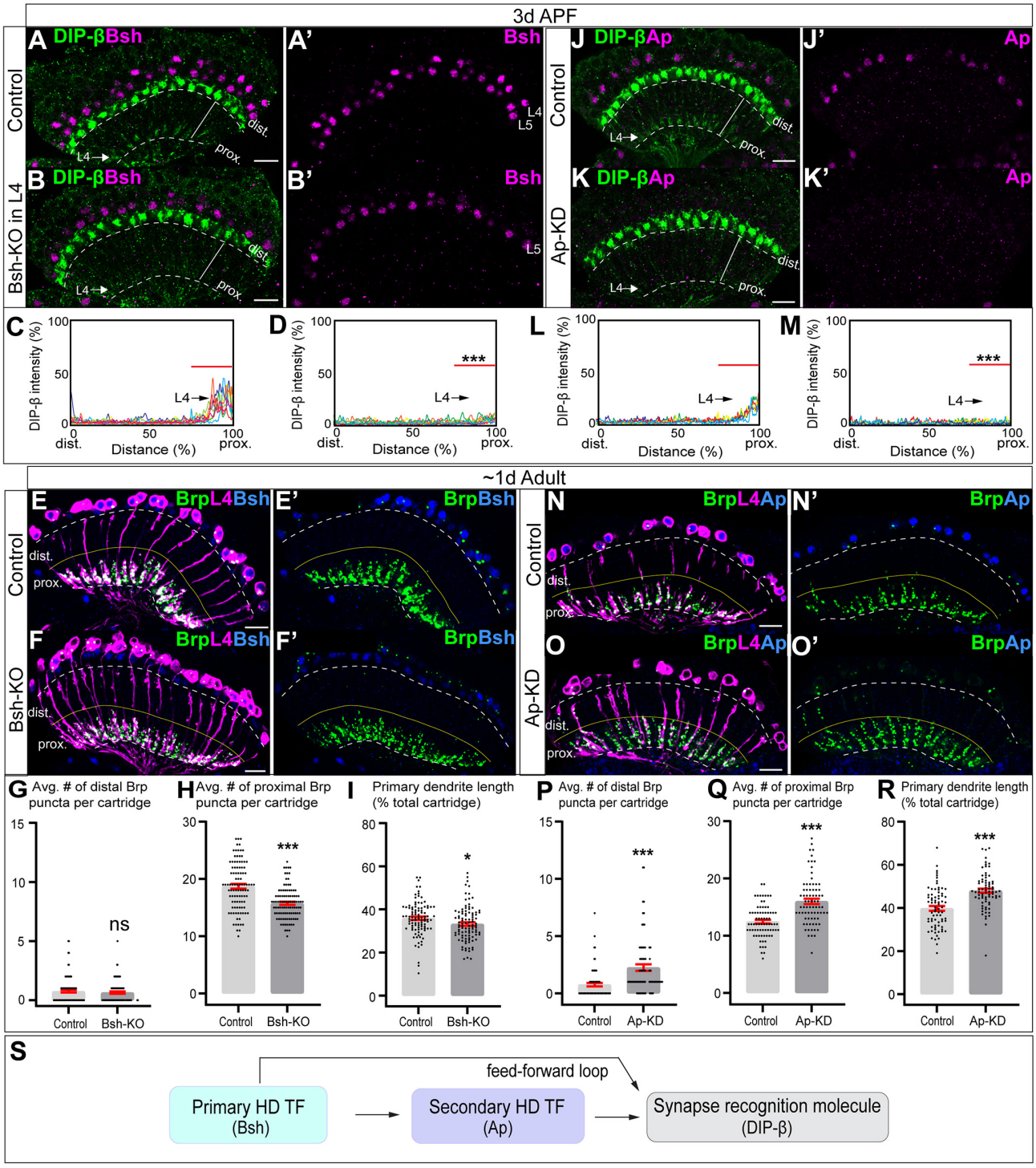


**Figure 5. Bsh and Ap are in a feed-forward loop that drives expression of the synapse recognition molecule DIP-β**

(A-D) Bsh Crispr KO in L4 neurons (31C06-AD, 34G07-DBD>UAS-Cas9, UAS-Bsh-sgRNAs) results in a loss of Bsh and DIP-β expression in L4. Note that DIP-β signal in the proximal lamina belongs to L4 in control (arrow, L4), whereas DIP-β signal in the distal lamina belongs to unknown

722 cells. Significantly reduced DIP-β fluorescence intensity is observed in the proximal lamina (75%–
723 100% distance, marked by red bar in (C) and (D)) of Bsh-KO flies (D) compared to control (C).
724 ***$P$<0.001, unpaired t-test, n=8 brains, each line represents each brain, scale bar, 10 µm.
725 (E-I) Bsh-KO decreases primary dendrite length (I) and proximal synapse number (H) in L4 (31C06-
726 AD, 34G07-DBD>UAS-Cas9, UAS-Bsh-sgRNAs, UAS-myrGFP, UAS-RSR, Brp-rst-stop-rst-
727 smFPV5-2a-GAL4). Here and below, white dash lines indicate the lamina neuropil. The yellow lines
728 show the boundary between the distal and proximal lamina. The average number of Brp puncta in L4
729 neurons present within the distal or proximal halves of lamina cartridges. *$P$<0.05, ***$P$<0.001, ns=
730 not significant, unpaired t-test, n=100 cartridges, n=5 brains, each dot represents each cartridge, data
731 are presented as mean ± SEM.
732 (J-M) Ap-KD in L4 neurons (27G05-Gal4>UAS-ApRNAi) results in a loss of Ap and DIP-β
733 expression. (L and M) Quantification of DIP-β fluorescence intensity for control (L) and Ap-KD
734 (M). ***$P$<0.001, unpaired t-test, n=6 brains in (L) and n=5 brains in (M), each line represents each
735 brain, scale bar, 10 µm.
736 (N-R) Ap-KD increases L4 primary dendrite length (R) and synapse number (P and Q) in L4
737 (31C06-AD, 34G07-DBD>UAS-RSR, 79C23-S-GS-rst-stop-rst-smFPV5-2a-GAL4, UAS-Ap-
738 shRNA, UAS-myrGFP). ***$P$<0.001, unpaired t-test, n=100 cartridges, n=5 brains, each dot
739 represents each cartridge, data are presented as mean ± SEM.
740 See also Figures S3, S6A-S6C, and S9.

Fig. 6

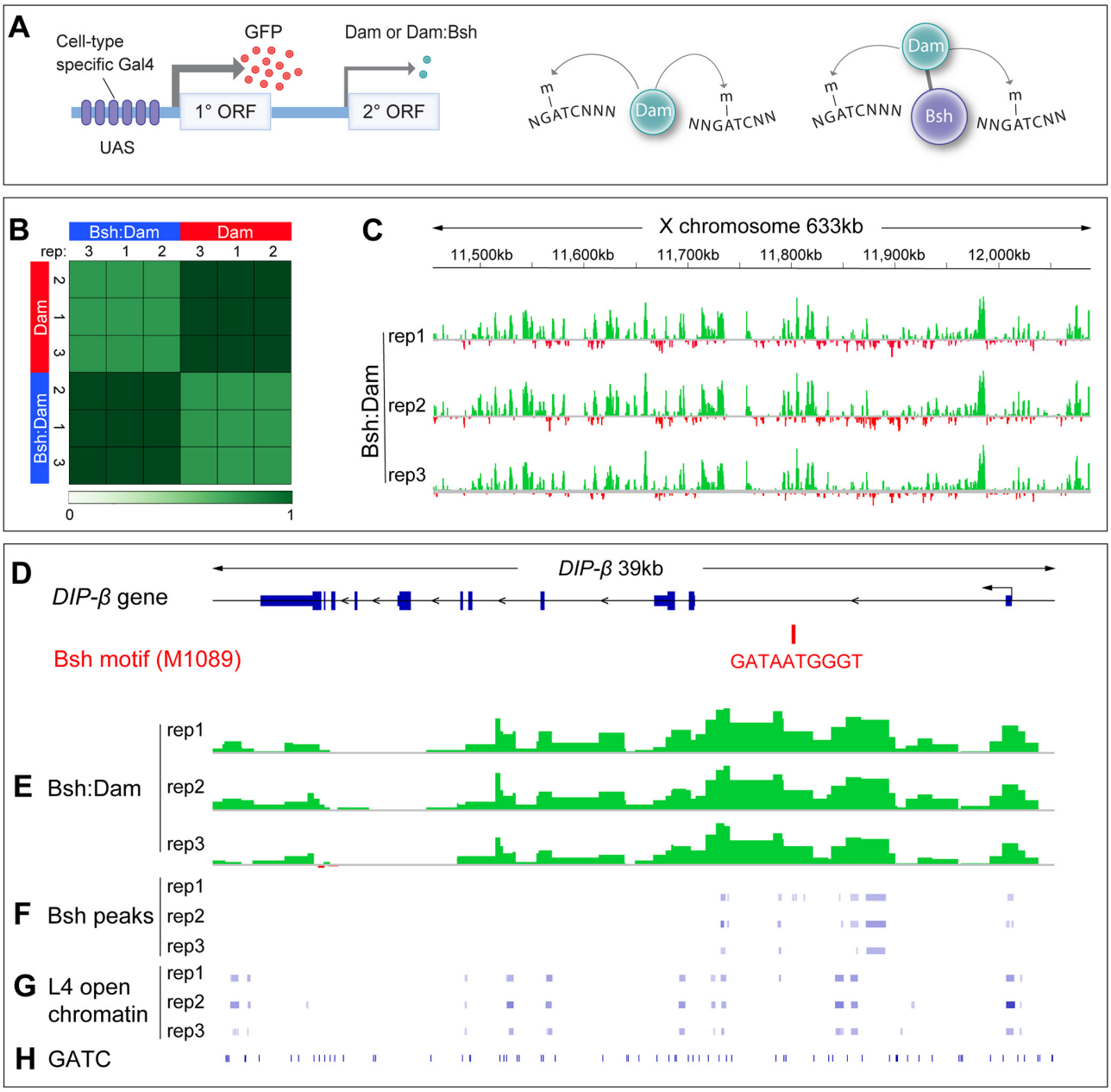


**Figure 6. *DIP-β* is a direct target of Bsh**

(A) Schematic for TaDa method.

(B) Three biological replicates of Dam and Bsh:Dam show high Pearson correlation coefficients.

(C) Bsh:Dam signal profiles over 633kb on chromosome X are highly similar in all three biological replicates. The y axes represent log2(Bsh:Dam/Dam) scores (data range for rep1: -2.04 to 5.01; rep2: -1.69 to 5.10 and rep3: -1.69 to 5.16).

(D) Bsh motif (M1089) is detected using PWM in the first intron of *DIP-β* gene.

(E) Bsh:Dam shows strong signals in the first intron of *DIP-β* gene. The y axes of Bsh:Dam signal represent log2(Bsh:Dam/Dam) scores (data range for rep1: -0.01 to 4.18; rep2: -0.13 to 4.53 and rep3: -0.36 to 4.33).
(F) Bsh binding peaks in L4 neurons were generated using MACS2 callpeak (the q-value cutoff: 0.001).
(G) L4 open chromatin peaks were generated using MACS2 callpeak (the q-value cutoff: 0.001).
(H) GATC sites available for Dam methylation.
See also Figure S10.

Fig. 7

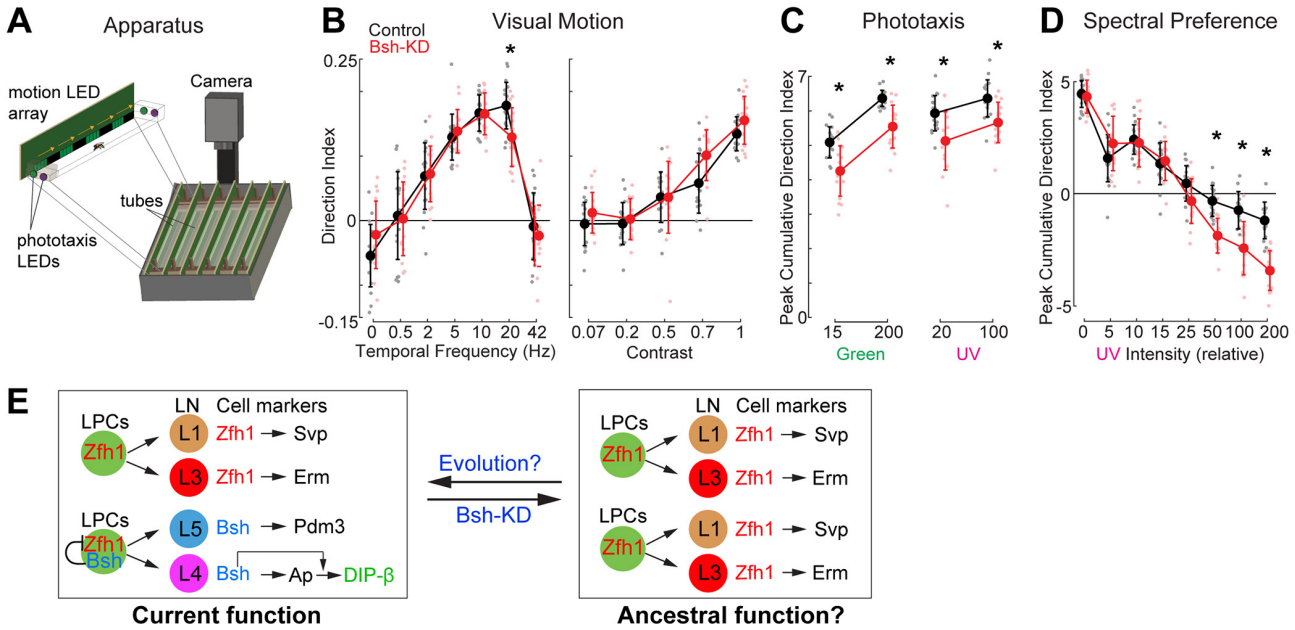


**Figure 7. Bsh+ L4/L5 are required for normal visual sensitivity**

(A) Schematic of the Fly Vision Box.

(B) Bsh-KD adult flies show reduced responses to a high-speed stimulus. Left: stimulus with different temporal frequency; right: stimulus with 5Hz temporal frequency, but with the indicated contrast level.

(C) Bsh-KD adult flies show reduced phototaxis to both dim and bright lights. Relative intensity was used: 15 and 200 for dim and bright green respectively; 20 and 100 for dim and bright UV respectively.

(D) Bsh-KD adult flies show larger responses towards bright UV illumination. For lower UV levels, flies walk towards the green LED, but walk towards the UV LED at higher UV levels.

(E) Model. Left: In wild type, Zfh1+ LPCs give rise to L1 and L3 neurons, whereas Zfh1+Bsh+ LPCs give rise to L4 and L5 neurons. The lineage relationship between these neurons is unknown. Right: Bsh KD results in transformation of L4/L5 into L1/L3 which may reveal a simpler, ancestral pattern of lamina neurons that contains the core visual system processing arrangement.

Data are presented as mean ± SD, with individual data points representing the mean value of all flies in each tube. For control (mcherry-RNAi), n=18 groups of flies (tubes), for Bsh-KD, n=16 groups of flies, run across 3 different experiments. Each group is 11-13 male flies. *$P$< 0.05, unpaired, two-sample t test controlled for false discovery rate.

See also Figures S2B and S11.

Fig. S1

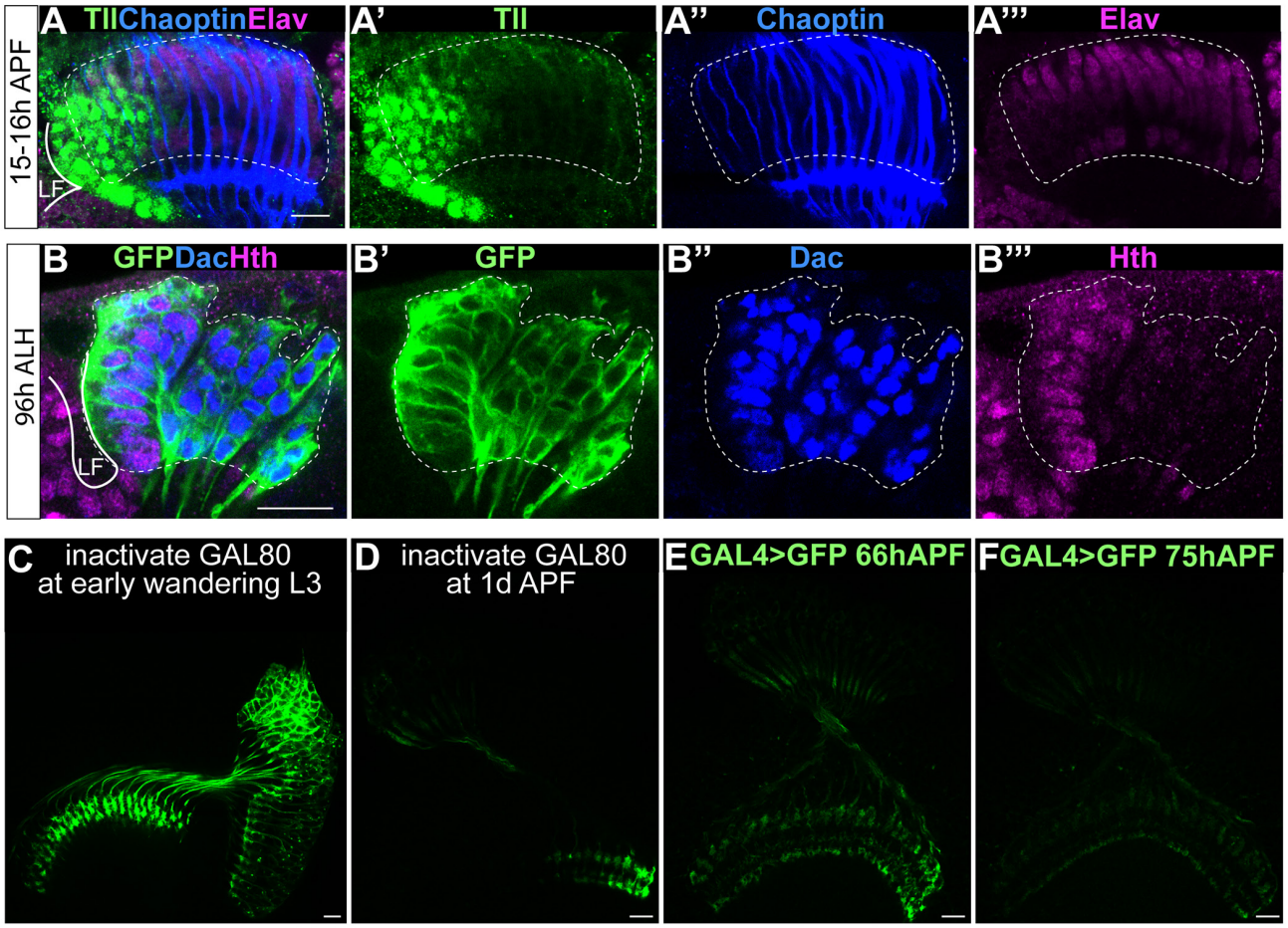


**Figure S1. Tll labels LPCs both within the lamina column and before the column; 27G05-GAL4 is turned on in all LPCs and turned off in lamina neurons.**

(A-A''') Tll+ cells are localized both within the lamina columns and before the columns. Lamina columns (white dash circle) are outlined by the photoreceptor axons which is labeled by Chaoptin. Here and below, scale bar, 10 µm. n≥5 brains. LF: lamina furrow.

(B-B''') 27G05-Gal4 drives GFP expression in all LPCs and lamina neurons (white dash circle) which are labeled by Dac at 96 hours after larval hatching (ALH). Hth labels LPCs next to lamina furrow (Piñeiro et al., 2014).

(C and D) 27G05-Gal4 is turned off in lamina neurons. GFP can be detected broadly in lamina neurons when Gal 80 is inactivated (27G05-Gal4 is activated) from the early stage of lamina neurogenesis (at early wandering L3) for 20 hours at 29.2 °C (27G05-Gal4>UAS-myrGFP, tubP-Gal80[ts]). GFP can be detected in very few lamina neurons when Gal 80 is inactivated (27G05-Gal4 is activated) close to the end of lamina neurogenesis (at 1d APF) for 20 hours at 29.2 °C (27G05-Gal4>UAS-myrGFP, tubP-Gal80[ts]).

(E and F) myrGFP (27G05-Gal4>UAS-myrGFP) can be detected in the cell bodies of lamina neurons until 66h APF and in the neurites until 75h APF though 27G05-Gal4 is turned off in lamina neurons.

Fig. S2

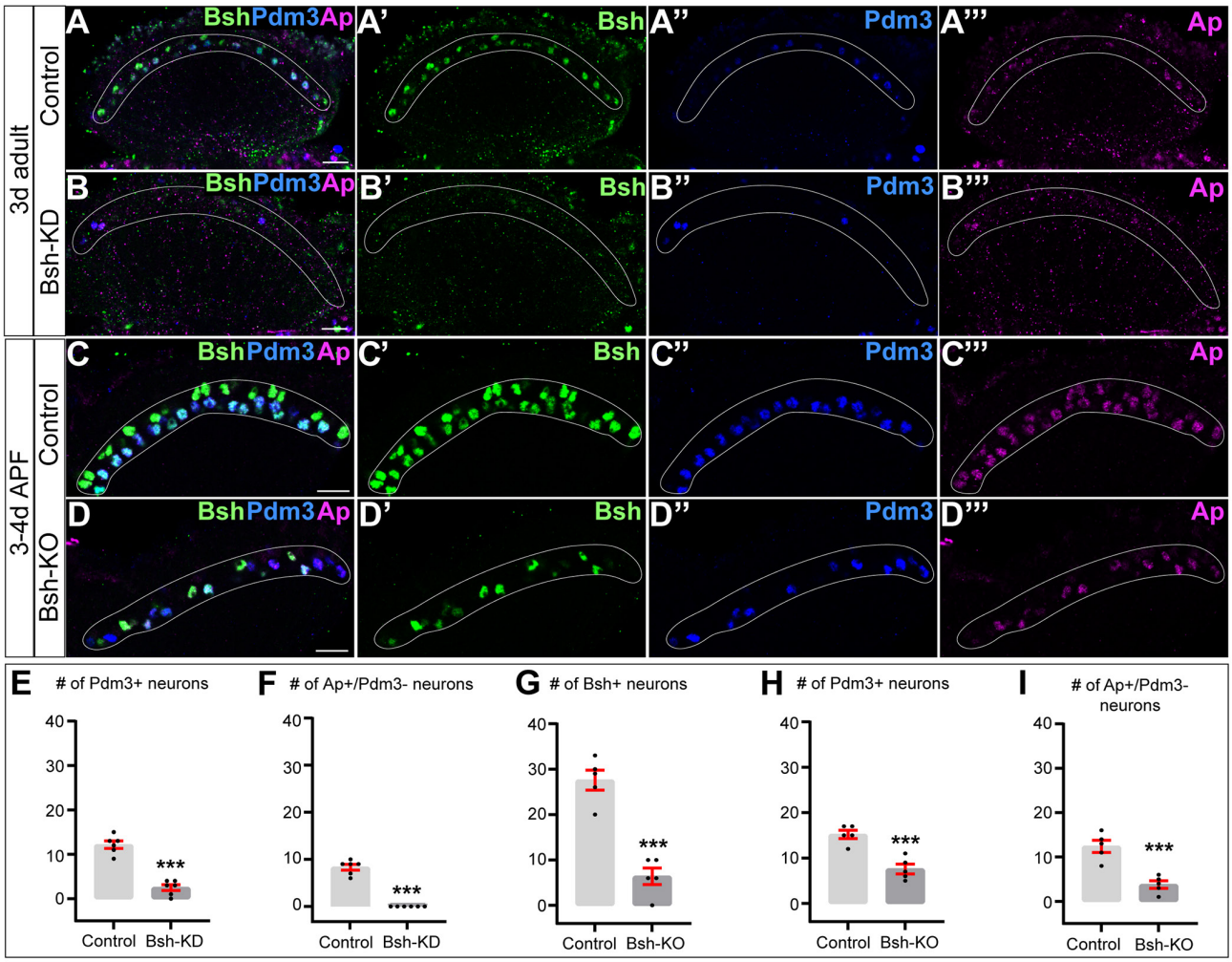


**Figure S2. Bsh-KD or Bsh-KO in LPCs affects L4/L5 neuronal fate.**

(A-B''') Bsh-KD in LPCs removes most L4 (Bsh/Ap) and L5 (Bsh/Pdm3) neuron markers. The Ap expression in L5 is caused by the Gal4 driver line but is irrelevant here. Here and below, scale bar, 10 µm, white circle outlines the region of L4 and L5 cell bodies.

(C-D''') Bsh-KO in LPCs (27G05-Gal4>UAS-Cas9, UAS-Bsh-sgRNAs) decreases Ap and Pdm3 expression in the lamina.

(E and F) The number of Pdm3+ (E) or Ap+/Pdm3- (F) cell bodies in single slice in control (A) and Bsh-KO (B).

(G-I) The number of Bsh+ (G), Pdm3+ (H) or Ap+/Pdm3- (I) cell bodies in single slice in control (C) and Bsh-KO (D).

Data are presented as mean ± SEM. Each dot represents each brain. n=6 brains in (E) and (F), n=5 brains in (G), (H), and (I). Each dot represents each brain. ***$P$<0.001, unpaired t-test.

Fig. S3

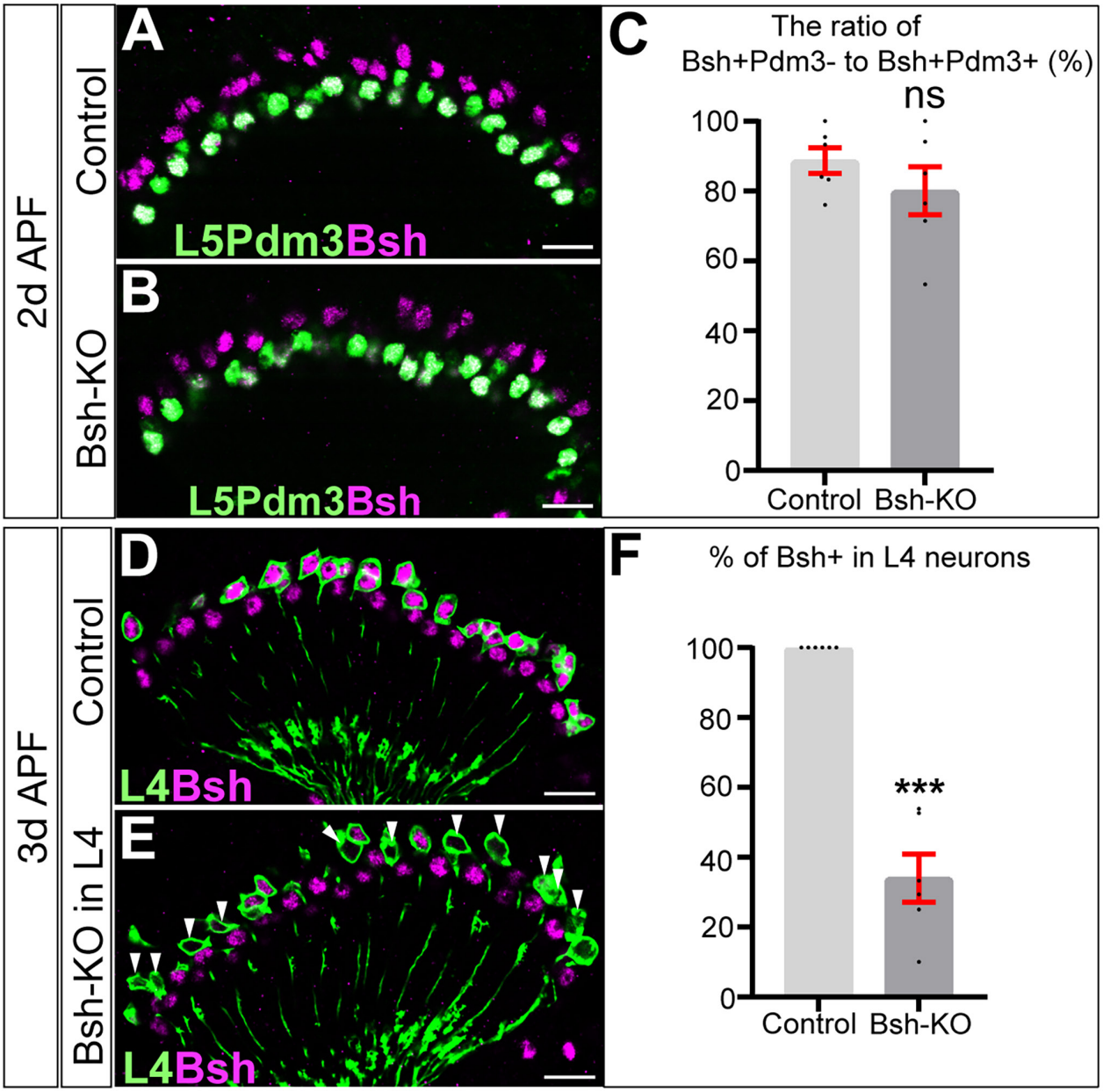


**Figure S3. Bsh becomes absent in some L4 neurons between 2d and 3d APF when knocking out Bsh in L4.**

(A-C) Bsh expression remains normal in L4 neurons at 2d APF when knocking out Bsh in L4 neurons (31C06-AD, 34G07-DBD>UAS-Cas9, UAS-Bsh-sgRNAs). Bsh+ Pdm3- labels L4 cell bodies. (C) The ratio of Bsh+ L4 (Bsh+/Pdm3-) and Bsh+ L5 (Bsh+/Pdm3+) in control (A) and Bsh-KO (B) at 2d APF.

(D -F) Bsh expression is absent in most L4 neurons when knocking out Bsh in L4 neurons (31C06-AD, 34G07-DBD>UAS-Cas9, UAS-Bsh-sgRNAs) at 3d APF. GFP (31C06-AD, 34G07-

817 DBD>UAS-myrGFP) labels L4 neurons. White arrowhead indicates L4 cell body lacking Bsh
818 expression. (F) The percentage of Bsh expression in L4 neurons (GFP+) at 3d APF.
819 Data are presented as mean ± SEM. ns= not significant, ***$P$<0.001, unpaired t-test, n= 6 brains in
820 (C) and (F), each dot represents each brain. Scale bar, 10 μm.

Fig. S4

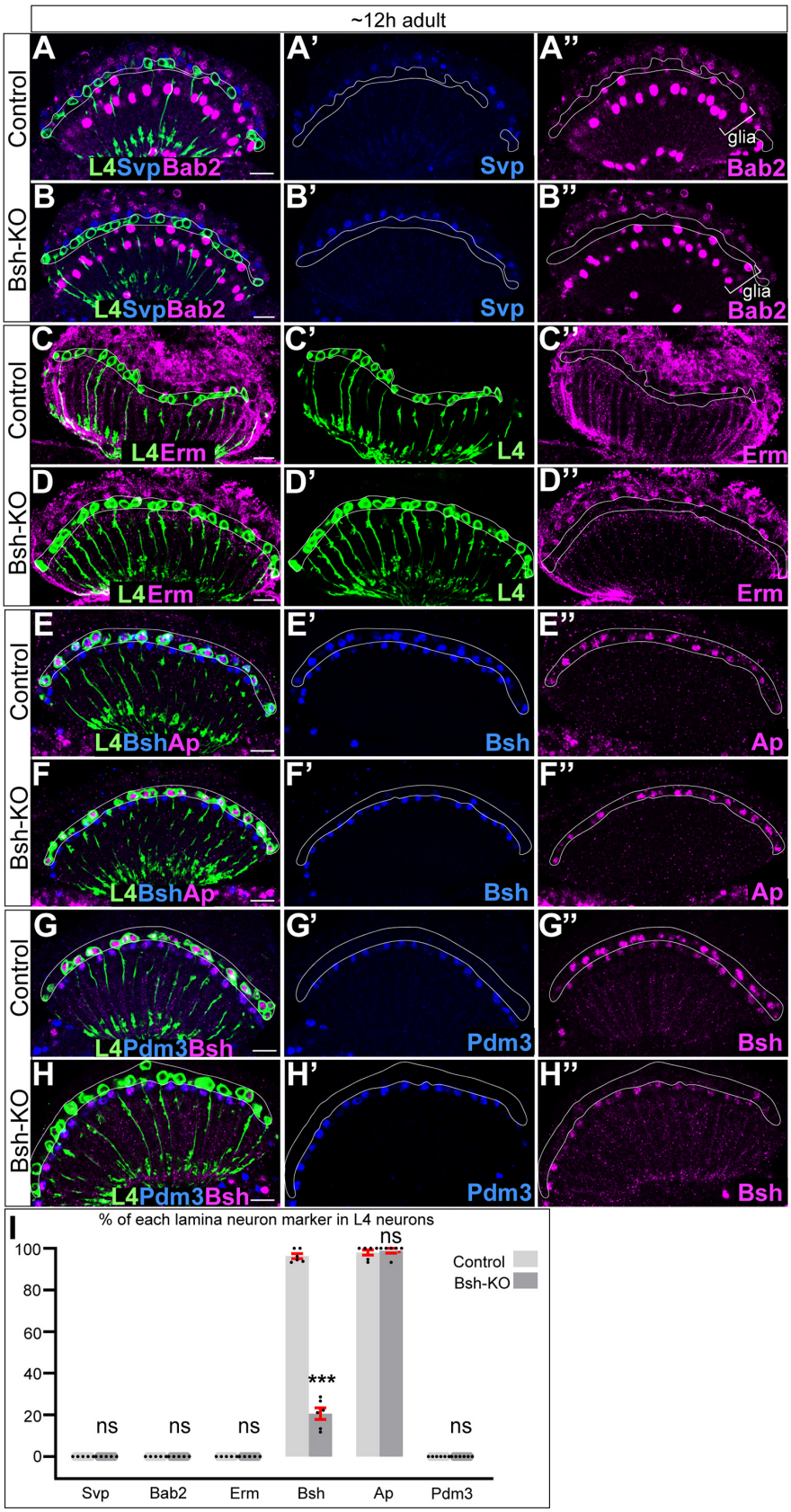
~12h adult
Control
Bsh-KO
A
A'
A''
L4SvpBab2
Svp
glia
Bab2
B
B'
B''
C
C'
C''
L4Erm
L4
Erm
D
D'
D''
E
E'
E''
L4BshAp
Bsh
Ap
F
F'
F''
G
G'
G''
L4Pdm3Bsh
Pdm3
H
H'
H''
I
% of each lamina neuron marker in L4 neurons
100
80
60
40
20
0
ns
***
Control
Bsh-KO
Svp
Bab2
Erm
Bsh
Ap
Pdm3

821

822 **Figure S4. Bsh is not required in L4 neurons to maintain L4 neuronal fate.**
823 (A-B'') L1 marker Svp and L2 marker Bab2 are not detected in L4 cell bodies when knocking out
824 Bsh in L4 (31C06-AD, 34G07-DBD>UAS-Cas9, UAS-Bsh-sgRNAs). Here and below, L4 is labeled
825 by GFP (31C06-AD, 34G07-DBD> UAS-myrGFP). White outline, L4 cell body. Scale bar, 10 µm.
826 (C-D'') L3 marker Erm is not detected in L4 cell bodies when knocking out Bsh in L4.
827 (E-F'') Bsh becomes absent in most L4 while Ap expression remains normal when knocking out Bsh
828 in L4.
829 (G-H'') L5 marker Pdm3 is not detected in L4 cell bodies when knocking out Bsh in L4.
830 (I) The percentage of each lamina neuron marker in L4 neurons (GFP+). ***$P$<0.001, ns= not
831 significant, unpaired t-test, n= 5 or 6 brains, each dot represents each brain, data are presented as
832 mean ± SEM.

Fig. S5

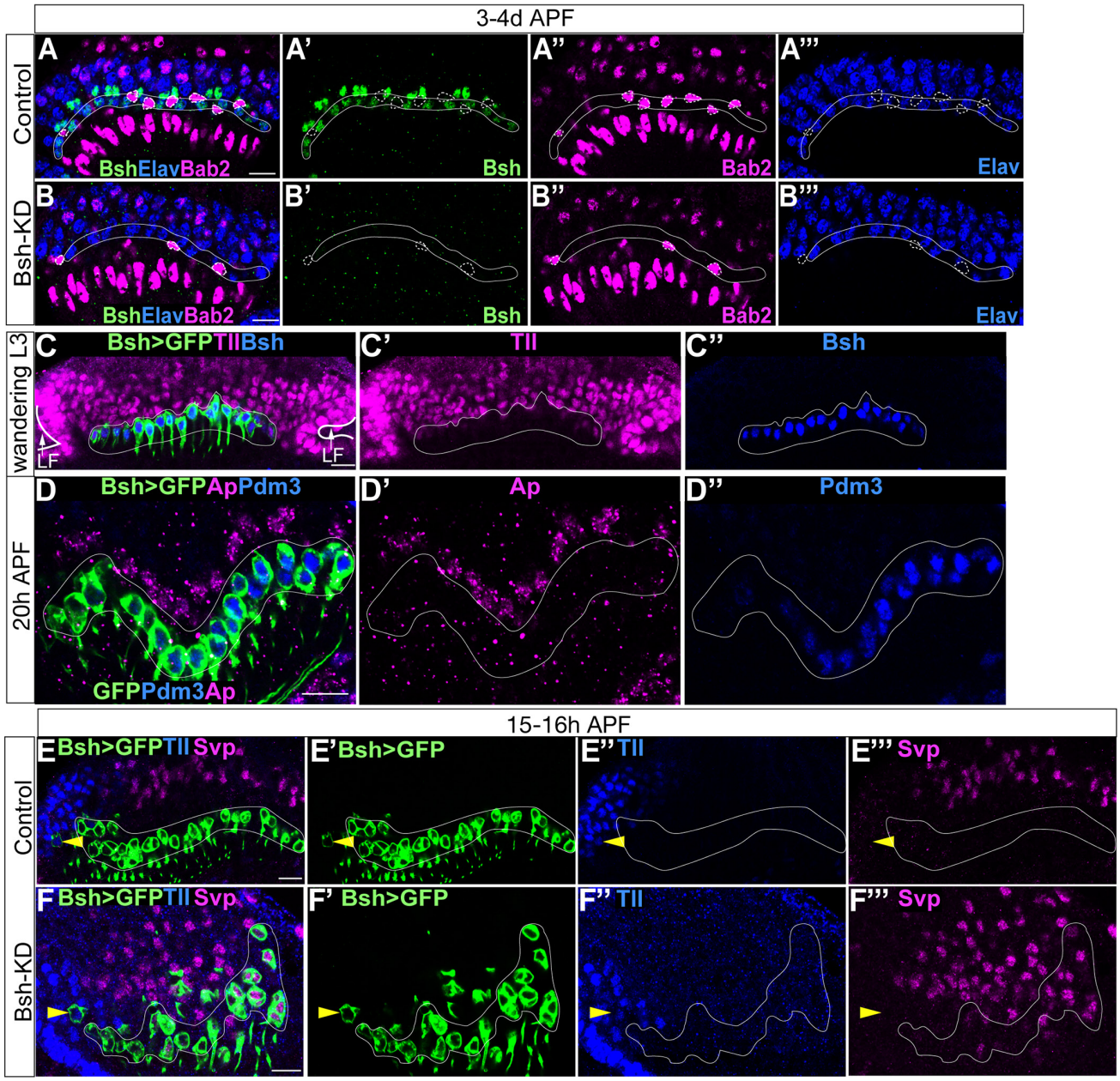


**Figure S5. L1 neurons are ectopically generated at the expense of L5 neurons when knocking down Bsh in LPCs.**

(A-B''') Bsh-KD in LPCs (27G05-Gal4>UAS-Bsh-RNAi) does not produce ectopic Bab2-positive L2 neurons. Bsh is absent in Bsh-KD. Bab2-positive cell bodies with white dash circles are glia. White circle outlines L5 cell body layer. Here and below, scale bar, 10 µm, n≥5 brains.

(C-C'') Bsh-LexA drives LexAop-myrGFP expression in Bsh+ LPCs and Bsh+ neurons. Tll labels lamina LPCs. White circle outlines GFP+ cells.

(D-D'') Bsh-LexA drives LexAop-myrGFP expression in L5 neurons but not L4 at 20h APF. Older GFP cell bodies express L5 marker Pdm3. Ap labels L4 neurons. White circle outlines GFP+ cells.

843 (E-F’’’) L1 marker Svp is ectopically expressed in GFP+ neurons but not GFP+ LPCs in Bsh-KD.
844 GFP labels LPCs and L5 neurons in control (Bsh-LexA>LexAop-myrGFP); Tll labels LPCs. White
845 line circle outlines GFP+ neurons. GFP+ LPCs are Tll positive (yellow arrowhead).

Fig. S6

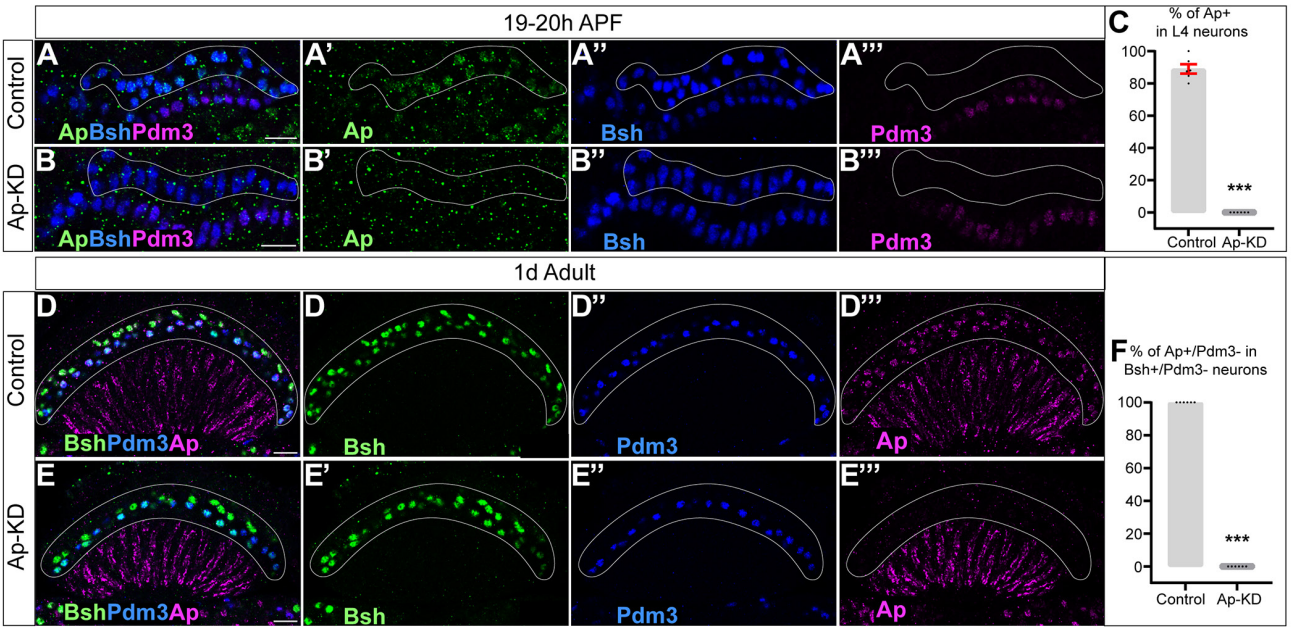


**Figure S6. Ap-KD eliminates Ap initiation and maintenance in L4 neurons.**

(A-C) Ap initiation in L4 neurons is eliminated at 19-20h APF when knocking down Ap (27G05-GAL4>UAS-Ap-RNAi). The top Bsh+ labels L4 and the bottom Bsh+ labels L5. Ap and Pdm3 are expressed in older L4 and older L5 neurons respectively. The Ap expression in L5 neurons is caused by the Gal4 driver line but is irrelevant here. Scale bar, 10 µm. (C) The percentage of Ap expression in L4 neurons (top Bsh+ row) in control (A) and Ap-KD (B).

(D-F) Ap expression remains undetectable in adult though Bsh expression remains normal. Bsh is unlikely able to reinitiate Ap expression if normal Ap initiation is lost. Scale bar, 10 µm. (F) The percentage of Ap expression (Ap+/Pdm3-) in L4 neurons (Bsh+/Pdm3-) in control (D) and Ap-KD (E).

Data are presented as mean ± SEM. Each dot represents each brain. n=6 brains in (C) and (F). ***$P$<0.001, unpaired t-test.

Fig. S7

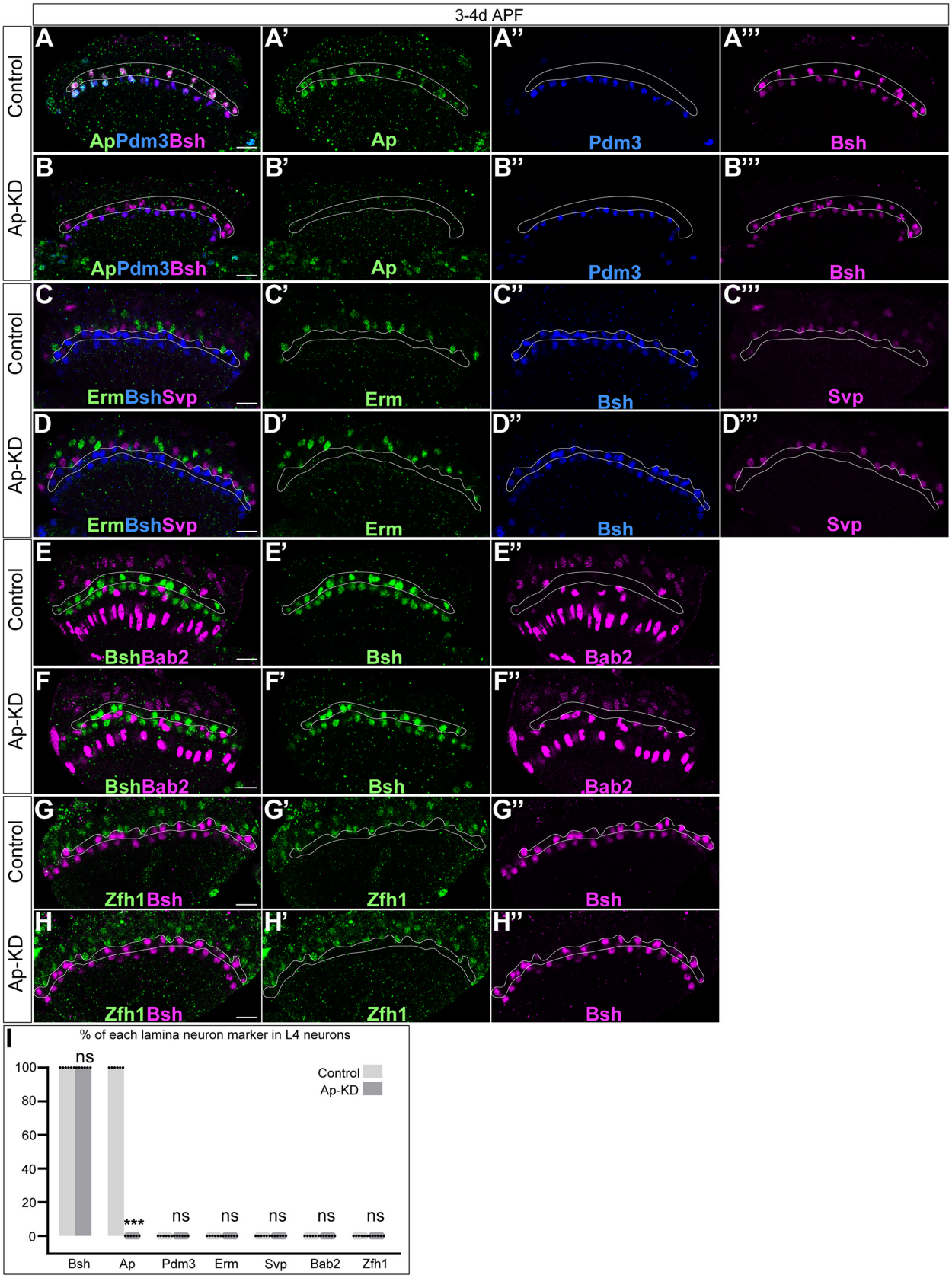
3-4d APF
Control
Ap-KD
A
ApPdm3Bsh
A'
Ap
A''
Pdm3
A'''
Bsh
B
ApPdm3Bsh
B'
Ap
B''
Pdm3
B'''
Bsh
C
ErmBshSvp
C'
Erm
C''
Bsh
C'''
Svp
D
ErmBshSvp
D'
Erm
D''
Bsh
D'''
Svp
E
BshBab2
E'
Bsh
E''
Bab2
F
BshBab2
F'
Bsh
F''
Bab2
G
Zfh1Bsh
G'
Zfh1
G''
Bsh
H
Zfh1Bsh
H'
Zfh1
H''
Bsh
I
% of each lamina neuron marker in L4 neurons
Control
Ap-KD
100
80
60
40
20
0
ns
***
ns
ns
ns
ns
ns
Bsh
Ap
Pdm3
Erm
Svp
Bab2
Zfh1

859

860 **Figure S7. Ap is not required to suppress other lamina neuron markers in L4 neurons.**
861 (A-H'') L1 (Svp, Zfh1), L2 (Bab2), L3 (Erm, Zfh1) and L5 (Pdm3) markers are not expressed in L4
862 neurons (top Bsh+ row) at 3-4d APF when knocking down Ap (27G05-GAL4>UAS-Ap-RNAi).
863 Scale bar, 10 µm.
864 (I) The percentage of each lamina neuron marker in L4 neurons (top row of Bsh+). ***$P$<0.001, ns=
865 not significant, unpaired t-test, n= 6 brains, each dot represents each brain, data are presented as
866 mean ± SEM.

Fig. S8

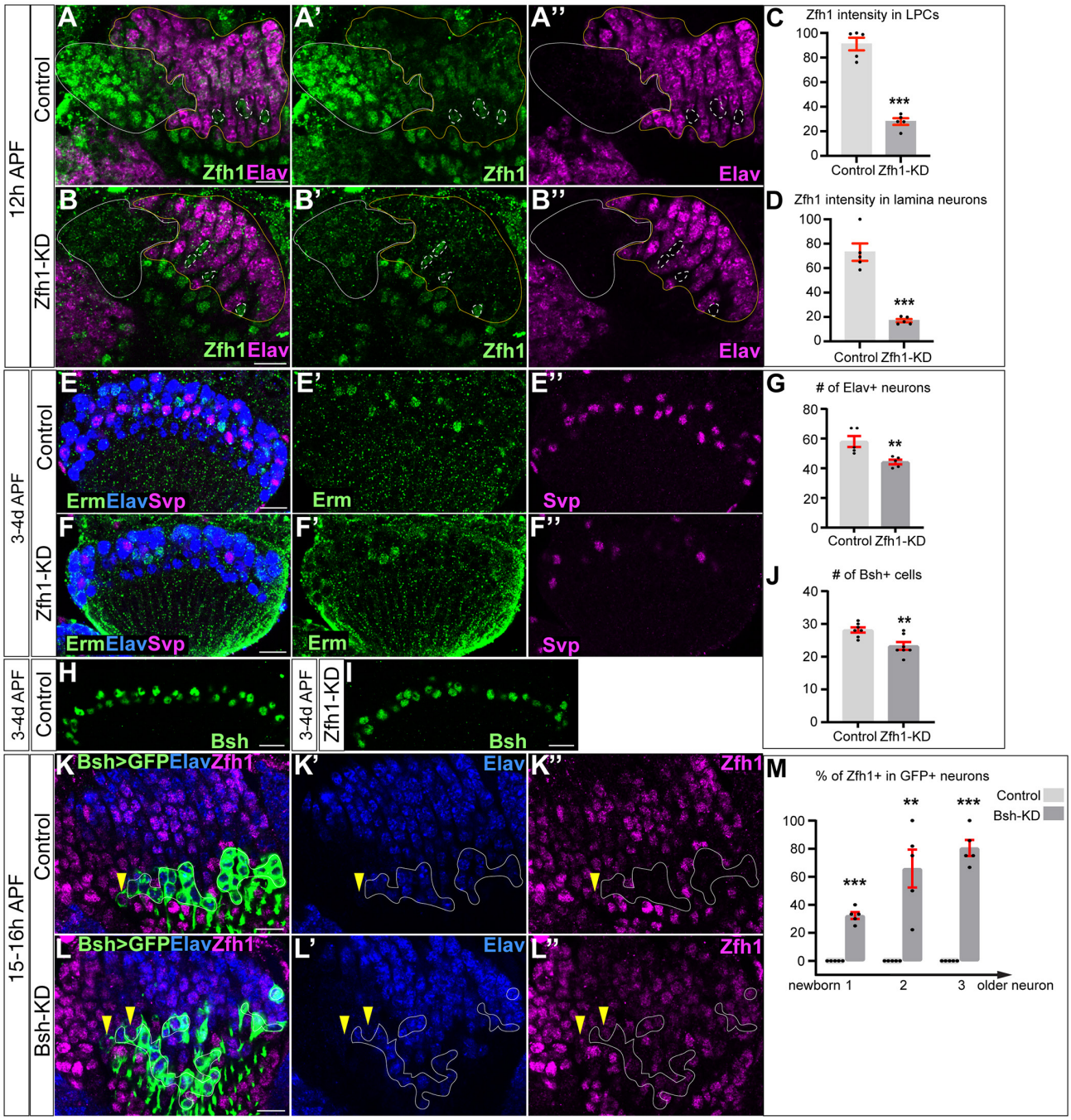


**Figure S8. Zfh1 knockdown in LPCs eliminates Zfh1 expression in all LPCs and neurons, and Zfh1 is ectopically expressed in Bsh-KD.**

(A-D) Zfh1-KD in LPCs (27G05-Gal4>UAS-Zfh1-RNAi) significantly reduces Zfh1 expression in all LPCs and lamina neurons at 12h APF. White line circle outlines LPCs. Yellow line circle outlines lamina neurons. White dash circle outlines glia with Zfh1 expression. Scale bar, 10 µm. (C and D) Quantification of Zfh1 signal in the cell bodies of LPCs (Elav-) (C) or neurons (Elav+) (D) in

control (A) and Zfh1-KD (B). We averaged the Zfh1 signal of three cells bodies from each brain and normalized Zfh1 signal by setting the highest Zfh1 signal as 100.

(E-G) The number of lamina neurons is decreased when knocking down Zfh1 in LPCs. Scale bar, 10 µm. (G) The number of Elav+ cells in single slice.

(H-J) The number of Bsh+ L4 and L5 neurons is decreased when knocking down Zfh1 in LPCs. Scale bar, 10 µm. (J) The number of Bsh+ L4 and L5 neurons in single slice.

(K-M) Zfh1 is ectopically expressed in GFP+ neurons. GFP (Bsh-LexA>LexAop-myrGFP) labels LPCs and L5 neurons in control. White line circle outlines GFP+ neurons. GFP+ LPCs are Tll+ (yellow arrowhead). Scale bar, 10 µm. (M) The percentage of Zfh1+ cells in GFP+ neurons (Tll-) in control (K) and Bsh-KD (L). We divided GFP+ neurons into three domains with equal width from the newborn to older neurons.

Data are presented as mean ± SEM. Each dot represents each brain. n=5 brains in (C), (D), (G), (J), and (M). Each dot represents each brain. $^{**}P<0.01$, $^{***}P<0.001$, unpaired t-test.

Fig. S9

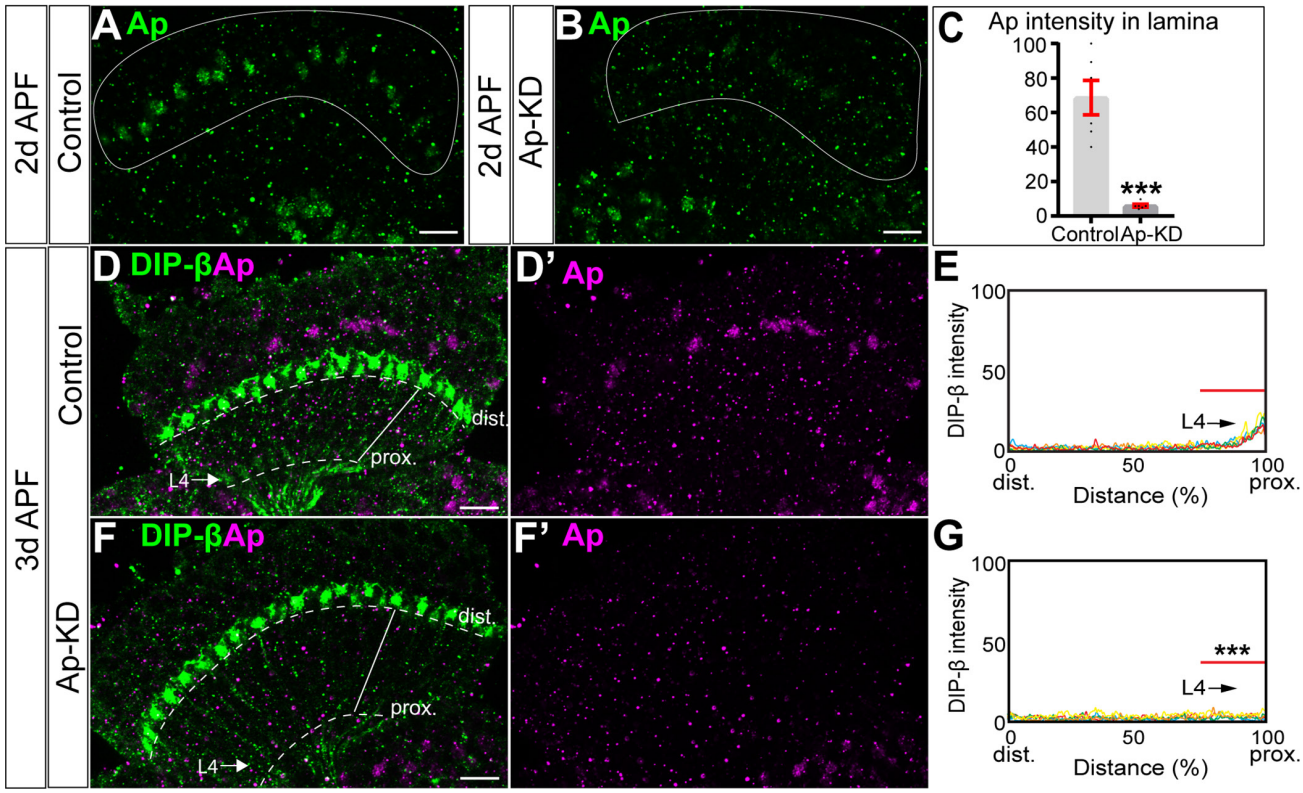


**Figure S9. DIP-β expression is disrupted when knocking down Ap in L4 neurons.**
(A and C) Ap-KD (31C06-AD, 34G07-DBD>UAS-RSR, 79C23-S-GS-rst-stop-rst-smFPV5-2a-GAL4, UAS-Ap-shRNA; see methods for an explanation of this genotype) significantly reduced Ap expression in L4 neurons at 2d APF. White line circle outlines lamina neuron cell bodies. Scale bar, 10 µm. (C) Quantification of Ap signal in the cell bodies of L4 neurons in control (A) and Ap-KD (B). We averaged the Ap signal of three cells bodies from each brain and normalized Ap signal by setting the highest Ap signal as 100. ***$P$<0.001, unpaired t-test, n= 6 brains, each dot represents each brain, data are presented as mean ± SEM.
(D and F) DIP-β expression is disrupted in L4 neurons in Ap-KD (31C06-AD, 34G07-DBD>UAS-RSR and 79C23-S-GS-rst-stop-rst-smFPV5-2a-GAL4) and UAS-Ap-shRNA. Note that DIP-β signal in the proximal lamina belongs to L4 in control (arrow, L4), whereas DIP-β signal in the distal lamina belongs to unknown cells. Scale bar, 10 µm.
(E and G) Quantification of DIP-β fluorescence intensity along the long axis of lamina cartridges (see white lines in (D) and (F)) from the distal dash line to the proximal dash line. Significantly reduced fluorescence intensity is observed in the proximal lamina (75%–100% distance, marked by red bar in (E) and (G)) of Ap-KD flies compared to control. ***$P$<0.001, unpaired t-test, n=5 brains, each line represents each brain.

Fig. S10

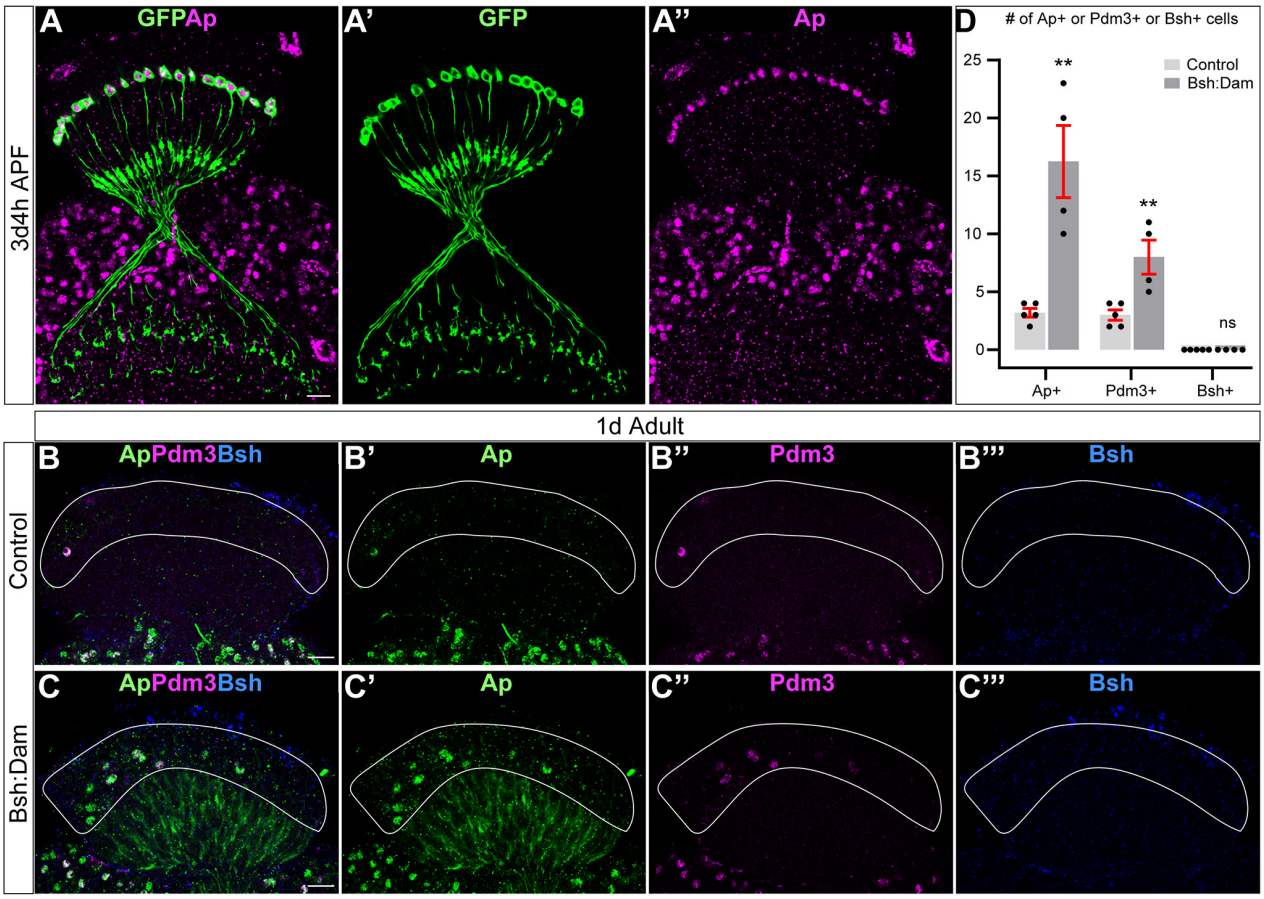


**Figure S10. Bsh:Dam is functional and 31C06-Gal4 is specifically expressed in L4 neurons between 1d46h APF and 3d4h APF**

(A-A'') GFP is expressed specifically in L4 neurons when activating 31C06-Gal4 for 24 hours at 29.2 °C (31C06-Gal4>UAS-myrGFP, tubP-Gal80[ts]). Here and below, scale bar, 10 µm.

(B-D) Bsh:Dam retains Bsh function and can partially rescue Ap and Pdm3 expressions in Bsh-KO flies (Bsh-KO; 27G05-Gal4>UAS-myrGFP-Bsh:Dam). Bsh:Dam expression is extremely low to avoid the toxicity and could not be detected by immunostaining. White circle outlines the cell body area of lamina neurons. (D) The number of Ap+ or Pdm3+ or Bsh+ cell bodies within z stack of 2.88 µm in control (B) and Bsh:Dam (C).

Fig. S11

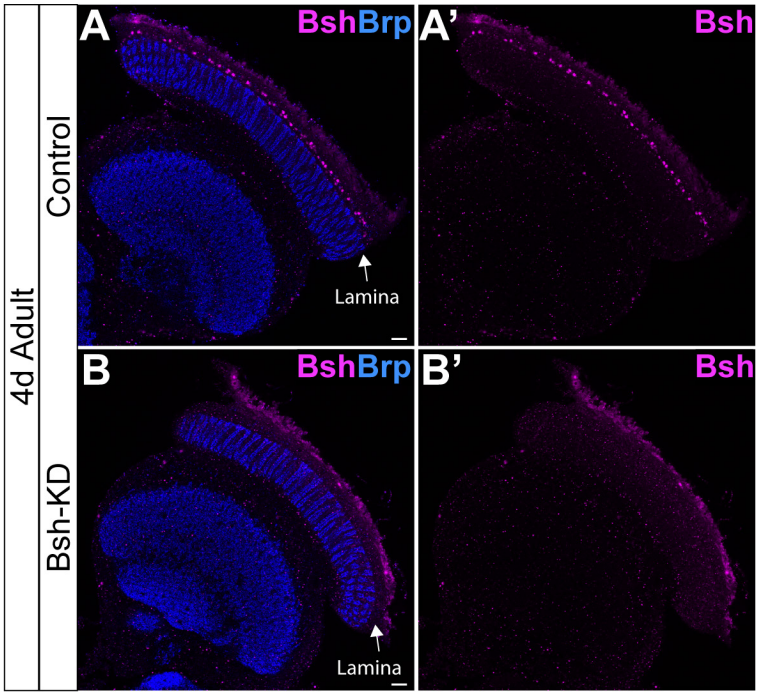


**Figure S11. Bsh expression is absent in the lamina of adult fly when knocking down Bsh in LPCs**

(A-B') Bsh is expressed in the lamina in control flies (A and A') (w+, 27G05-Gal4>UAS-mcherry-RNAi, tubP-Gal80[ts]) while its expression becomes absent in the lamina in Bsh-KD (B and B') (w+, 27G05-Gal4>UAS-Bsh-RNAi, tubP-Gal80[ts]) (see Methods). Brp labels the neuropils in the optic lobe of 4-day old adult fly at 29°C. Arrow: lamina. Scale bar, 10 µm.